International Journal of Heat and Mass Transfer 102 (2016) 944–958

Contents lists available at ScienceDirect

International Journal of Heat and Mass Transfer

journal homepage: www.elsevier.com/locate/ijhmt

Discrete unified gas kinetic scheme for multiscale heat transfer based on the phonon Boltzmann transport equation

Zhaoli Guo [a,*], Kun Xu [b]

[a] State Key Laboratory of Coal Combustion, Huazhong University of Science and Technology, Wuhan 430074, China
[b] Department of Mathematics, Hong Kong University of Science and Technology, Clear Water Bay, Hong Kong, China

ARTICLE INFO

Article history:
Received 11 March 2016
Accepted 25 June 2016

Keywords:
Discrete unified gas kinetic scheme
Phonon
Boltzmann transport equation
Multiscale heat transfer

ABSTRACT

Numerical prediction of multiscale heat transfer is a challenging problem due to the wide range of time and length scales involved. In this work a discrete unified gas kinetic scheme (DUGKS) is developed for heat transfer in materials with different acoustic thickness based on the phonon Boltzmann equation. With discrete phonon direction, the Boltzmann equation is discretized with a second-order finite-volume formulation, in which the time-step is fully determined by the Courant–Friedrichs–Lewy (CFL) condition. The scheme has the asymptotic preserving (AP) properties for both diffusive and ballistic regimes, and can present accurate solutions in the whole transition regime as well. The DUGKS is a self-adaptive multiscale method for the capturing of local transport process. Numerical tests for both heat transfers with different Knudsen numbers are presented to validate the current method.

1. Introduction

Many emerging nanostructures involve semiconductors and dielectrics, in which phonon transport is the main mechanism for heat transfer. Heat transfer process in systems with such nanostructures usually involves multiple temporal and spatial scales [1–3], and it is a challenging problem to develop efficient numerical methods that are applicable to different transport regimes. Owing to the breakdown of Fourier law at small time and spatial scales, and the high computational requirement of microscopic molecular dynamics, the phonon Boltzmann transport equation (BTE) [3,4] is regarded to be able to provide a good base for developing numerical methods for multiscale heat transfer when phase coherence effects are unimportant. Actually, many numerical schemes have been proposed to solve the BTE in previous studies [5], including the stochastic Monte-Carlo (MC) method [6–8] and the deterministic discrete ordinates method (DOM) coupled with finite-difference, finite-volume, or finite-element discretization of spatial space [9–13]. The lattice Boltzmann method (LBM), which was originally developed for continuous fluid flows [14], was also applied to phonon transport [15–18].

Generally, the MC method follows a time-splitting algorithm, namely, the dynamics of a simulated particle is decoupled into advection and scattering processes, and thus the time step used is less than the relaxation time, and the grid size is less than the phonon mean-free-path [19]. Consequently, the computational costs of MC method are expensive in the acoustic thick regime, which prohibit its applications for multiscale problems with diffusive region, although it can be quite efficient for ballistic transport. It is also noted that an improved MC method has been developed recently by simulating only the deviation from equilibrium such that the variance can be efficiently reduced in simulating systems with small temperature variations [8]. In the DOM method, the transient and advection terms in the BTE are usually discretized with techniques that are adopted in computational fluid dynamics (CFD), such as upwind (Step) and central (Diamond) finite-difference schemes, or finite-volume schemes with upwind interpolations. These CFD techniques may introduce significant artificial diffusions (low-order schemes) or numerical instability (high-order schemes) [5]. Regarding the LBM for phonon transport, although it has been applied to some nano and multiscale problems [15–18], some studies have shown that LBM may yield unphysical predictions [20].

Recently, a finite-volume discrete unified gas kinetic scheme (DUGKS) for molecule flows ranging from continuum to rarefied regimes has been developed [21,22], which has high accuracy and outstanding robustness. The nice asymptotic preserving (AP) properties also remove the restriction on the time step by the relaxation time that exists in other kinetic methods with direct discretization of the kinetic equation. Furthermore, the finite-volume formulation enables the DUGKS to handle problems with complex

* Corresponding author.
E-mail addresses: zlguo@hust.edu.cn (Z. Guo), makxu@ust.hk (K. Xu).

http://dx.doi.org/10.1016/j.ijheatmasstransfer.2016.06.088
0017-9310/

geometries [23]. Some comparative studies suggest that the DUGKS has better performances over the LBM even for continuum flows [24,25]. In this work, we will extend the DUGKS to phonon transport to construct an efficient method for the whole multiscale heat transport process ranging from diffusive to ballistic regimes.

The remainder of the paper is organized as follows. Section 2 gives a brief introduction of the phonon BTE, and the DUGKS for the BTE is described in Section 3. Some numerical simulations are carried out in Section 4 to test the scheme, and finally a brief summary is given in Section 5.

2. Phonon Boltzmann transport equation

In a rigid crystalline solids, the atomic vibrations from equilibrium positions can be quantized as quasi-particles known as phonons, and the system can be considered as a domain filled with a phonon gas. The angular frequency ω of a phonon is related to the wave number $\boldsymbol{k} \in R^3$ through certain dispersion relations $\omega = \omega_p(\boldsymbol{k})$, with different polarizations or modes of the phonon. The phonon transport can be described by the Boltzmann transport equation in the regime as the wave effects or phase coherence effects are negligible [2],

$$\frac{\partial f_p}{\partial t} + \boldsymbol{v}_p \cdot \nabla f_p = Q_p, \tag{1}$$

where $f_p = f_p(\boldsymbol{x}, \boldsymbol{k}, \boldsymbol{s}, t)$ (or $= f_p(\boldsymbol{x}, \omega, \boldsymbol{s}, t)$) is the distribution function dependent on wave number $\boldsymbol{k}$ (or frequency ω), polarization p, direction $\boldsymbol{s}$, and position $\boldsymbol{x}$ as well as time t; $\boldsymbol{v}_p = \partial\omega/\partial\boldsymbol{k}$ is the group velocity with which the phonon of polarization p travels. The term on the right hand side, Q_p, represents the rate of change of f_p due to scattering interactions. Usually the scattering is very complicated [3], and a more tractable model widely used is the relaxation time approximation,

$$Q_p = -\frac{1}{\tau_p}\left[f_p - f_p^{eq}\right], \tag{2}$$

where τ_p is the relaxation time, f_p^{eq} is the equilibrium distribution of phonons and follows the Bose–Einstein distribution,

$$f_p^{eq} = \frac{1}{\exp\left(\hbar\omega/k_B T\right) - 1}, \tag{3}$$

with $\hbar$ being the Planck's constant divided by 2π and k_B the Boltzmann constant, respectively, and T is the temperature defined later. The effective relaxation time τ_p usually depends on temperature and frequency, and can be estimated using the Matthiessen's rule if the individual scattering processes are independent of each other [1,26],

$$\frac{1}{\tau_p} = \frac{1}{\tau_U} + \frac{1}{\tau_N} + \frac{1}{\tau_b} + \frac{1}{\tau_i} + \cdots, \tag{4}$$

where the relaxation times appearing on the right hand side are those due to the umklapp (U) and normal (N) phonon–phonon scatterings, boundary scattering, impurity scattering, etc. With the effective relaxation time, one can define the Knudsen number of the system, $\mathrm{Kn} = \lambda_0/l_0$, where l_0 is the characterize length of the system, and $\lambda_0 = v_0\tau_0$ is the phonon mean free path with v_0 being a typical value of the phonon group velocity and τ_0 a typical value of the relaxation time.

The total energy and the heat flux can be defined from the phonon distribution function [27],

$$E = \sum_{\boldsymbol{k},p} \hbar\omega(\boldsymbol{k}) f_p(\boldsymbol{k}) = \sum_p \int_{4\pi} \int \hbar\omega f_p(\omega) D_p(\omega) d\omega d\Omega, \tag{5}$$

$$\boldsymbol{q} = \sum_{\boldsymbol{k},p} \hbar\omega(\boldsymbol{k}) \boldsymbol{v}_p(\boldsymbol{k}) f_p(\boldsymbol{k}) = \sum_p \int_{4\pi} \int \hbar\omega \boldsymbol{v}_p f_p(\omega) D_p(\omega) d\omega d\Omega, \tag{6}$$

where $D_p(\omega)$ is the density of state, and Ω is the solid angle. The temperature T of the system can be obtained from $T = E/C_V$, with C_V being the volume specific heat capacity.

Even with the relaxation time approximation, the BTE is still very difficult to be solved due to the high dimensionality. A number of tractable models have emerged to reduce the complex, such as gray model, semi-gray model, non-gray model, and phonon radiative transfer model [1,28]. To illustrate the essence of our numerical method clearly without loss of generality, we will consider the gray model with the Debye's linear dispersion relation in the present work. This simplified model assumes phonons of all polarizations and frequencies are same and the group speed v_g is a constant and the BTE (1) is expressed in terms of the phonon energy density $e''(\boldsymbol{x}, \boldsymbol{s}, t)$ [1],

$$\frac{\partial e''}{\partial t} + \boldsymbol{v} \cdot \nabla e'' = Q \equiv -\frac{1}{\tau}[e'' - e^{eq}], \tag{7}$$

where $\boldsymbol{v} = v_g \boldsymbol{s}$ is the group velocity, τ is the singlet relaxation time, and e'' is the reduced distribution function for energy density,

$$e''(\boldsymbol{x}, \boldsymbol{s}, t) = \sum_p \int \hbar\omega f_p(\omega) D_p(\omega)\, d\omega. \tag{8}$$

Obviously, the total phonon energy E and heat flux $\boldsymbol{q}$ can be determined from e'',

$$E = \int_{4\pi} e''(\boldsymbol{x}, \boldsymbol{s}, t)\, d\Omega, \quad \boldsymbol{q} = \int_{4\pi} \boldsymbol{v} e''(\boldsymbol{x}, \boldsymbol{s}, t)\, d\Omega. \tag{9}$$

The equilibrium distribution function e^{eq} is just the angular average of the total energy,

$$e^{eq}(\boldsymbol{x}, t) = \frac{1}{4\pi}\int_{4\pi} e''(\boldsymbol{x}, \boldsymbol{s}, t)\, d\Omega = \frac{E}{4\pi}. \tag{10}$$

The gray model employs a single phonon group speed v in all directions and a single relaxation time τ independent of polarization and frequency. Despite the simple formulation, the gray model can provide some insightful predictions on the phonon transport behaviors with acceptable accuracy, especially for low-thermal conductivity dielectrics [13,12]. In the diffusive limit ($\mathrm{Kn} \to 0$), it can be shown that the solution of the kinetic Eq. (7) is determined by its average E that obeys the diffusion equation (see Appendix A for details),

$$\frac{\partial E}{\partial t} = \nabla \cdot (\kappa \nabla T), \tag{11}$$

where the thermal conductivity is given by

$$\kappa = \frac{1}{3} C_V v_g^2 \tau. \tag{12}$$

3. Numerical scheme

3.1. Updating rule in finite-volume formulation

Now we present the construction of the discrete unified gas kinetic scheme (DUGKS) for phonon transport based on Eq. (7). First, the continuous solid angle domain Ω is discretized into N discrete angles using the discrete-ordinates method (DOM) based on certain spherical quadratures, and correspondingly we obtain N discrete directions $\boldsymbol{s}_i$. The accuracy of the quadrature employed is required to ensure the exact evaluation of the angular moments of the distribution function up to certain orders, such as

$$\sum_{\alpha=1}^{N} w_\alpha e''(\boldsymbol{s}_\alpha) = \int_{4\pi} e''(\boldsymbol{s}) d\Omega = E, \tag{13a}$$

$$\sum_{\alpha=1}^{N} w_\alpha e^{eq}(\boldsymbol{s}_\alpha) = \int_{4\pi} e^{eq}(\boldsymbol{s}) d\Omega = E, \tag{13b}$$

$$\sum_{\alpha=1}^{N} w_\alpha \boldsymbol{v}_\alpha e''(s_\alpha) = \int_{4\pi} \boldsymbol{v} e''(\boldsymbol{s}) d\Omega = \boldsymbol{q}, \tag{13c}$$

$$\sum_{\alpha=1}^{N} w_\alpha \boldsymbol{v}_\alpha e^{eq}(s_\alpha) = \int_{4\pi} \boldsymbol{v} e^{eq}(\boldsymbol{s}) d\Omega = 0, \tag{13d}$$

$$\sum_{\alpha=1}^{N} w_\alpha \boldsymbol{v}_\alpha \boldsymbol{v}_\alpha e^{eq}(s_\alpha) = \int_{4\pi} \boldsymbol{v}\boldsymbol{v} e^{eq}(\boldsymbol{s}) d\Omega = \frac{v_g^2}{3} E\boldsymbol{I}, \tag{13e}$$

where w_α and $\boldsymbol{s}_\alpha$ are the weights and the discrete angles of the corresponding spherical quadrature, $\boldsymbol{v}_\alpha = v_g \boldsymbol{s}_\alpha$ is the discrete group velocity, and $\boldsymbol{I}$ is the second-order unit tensor. These requirements suggest that the weights and the discrete angles satisfy

$$\sum w_\alpha = 4\pi, \quad \sum w_\alpha \boldsymbol{v}_\alpha = \boldsymbol{0}, \quad \sum w_\alpha \boldsymbol{v}_\alpha \boldsymbol{v}_\alpha = \frac{4\pi}{3}\boldsymbol{I}. \tag{14}$$

With the discrete directions, the BTE (7) can then be expressed as

$$\frac{\partial \phi_\alpha}{\partial t} + \boldsymbol{v}_\alpha \cdot \nabla \phi_\alpha = Q_\alpha \equiv -\frac{1}{\tau}(\phi_\alpha - \phi_\alpha^{eq}), \tag{15}$$

for $\alpha = 1, 2, \ldots, N$, where $\phi_\alpha(\boldsymbol{x}, t) = e''(\boldsymbol{x}, s_\alpha, t)$ and $\phi_\alpha^{eq}(\boldsymbol{x}, t) = e^{eq}(\boldsymbol{x}, s_\alpha, t)$. The total energy density and heat flux are then evaluated from the discrete distribution function for the phonon energy,

$$E = \sum_{\alpha=1}^{N} w_\alpha \phi_\alpha, \quad \boldsymbol{q} = \sum_{\alpha=1}^{N} w_\alpha \boldsymbol{v}_\alpha \phi_\alpha, \tag{16}$$

The DUGKS method developed here is a finite-volume scheme for solving the BTE (15), in which the spatial domain is divided into a set of control volumes. A one-dimensional (1D) and two-dimensional (2D) diagrams are shown in Fig. 1 as an example. Integrating Eq. (15) in the volume V_j centered at $\boldsymbol{x}_j$ from time t_n to $t_{n+1} = t_n + \Delta t$ leads to the following balance equation,

$$\phi_{\alpha j}^{n+1} - \phi_{\alpha j}^{n} + \frac{\Delta t}{|V_j|} \boldsymbol{F}_{\alpha j}^{n+1/2} = \frac{\Delta t}{2}\left[Q_{\alpha j}^{n+1} + Q_{\alpha j}^{n}\right], \tag{17}$$

where we have used the trapezoidal quadrature for the time integration of the collision term, and the mid-point rule for the flux term. $|V_j|$ is the volume of cell j. Here,

$$\boldsymbol{F}_{\alpha j}^{n+1/2} = \sum_{\boldsymbol{x}_b \in \mathcal{N}_j} (\boldsymbol{v}_\alpha \cdot \boldsymbol{n}_b) \phi_\alpha(\boldsymbol{x}_b, t_{n+1/2}) S(\boldsymbol{x}_b) \tag{18}$$

is the flux across the interfaces of cell j, where $\mathcal{N}_j$ is the set consisting of the centers of cell interfaces, $\boldsymbol{n}_b$ is the outward unit normal vector at $\boldsymbol{x}_b$ of an interface, and $S(\boldsymbol{x}_b)$ is the corresponding interface area. In Eq. (17), $\phi_{\alpha j}$ and $Q_{\alpha j}$ are the cell-averaged values of the distribution function and collision term, respectively,

$$\phi_{\alpha j} = \frac{1}{|V_j|}\int_{V_j} \phi_\alpha(\boldsymbol{x}, t)\, d\boldsymbol{x}, \quad Q_{\alpha j} = \frac{1}{|V_j|}\int_{V_j} Q_\alpha(\boldsymbol{x}, t)\, d\boldsymbol{x}. \tag{19}$$

The scheme (17) is implicit due to the inclusion of Q_α^{n+1} and the flux at half-time step $\boldsymbol{F}_\alpha^{n+1/2}$. Like in the original DUGKS for gas flows [21,22], the implicitness of the collision term can be removed by introducing a new distribution function defined as

$$\tilde{\phi}_\alpha = \phi_\alpha - \frac{\Delta t}{2} Q_\alpha = \frac{2\tau + \Delta t}{2\tau}\phi_\alpha - \frac{\Delta t}{2\tau}\phi_\alpha^{eq}, \tag{20}$$

or

$$\phi_\alpha = \frac{2\tau}{2\tau + \Delta t}\tilde{\phi}_\alpha + \frac{\Delta t}{2\tau + \Delta t}\phi_\alpha^{eq}. \tag{21}$$

Then Eq. (17) can be rewritten in terms of $\tilde{\phi}_\alpha$ as

$$\tilde{\phi}_{\alpha j}^{n+1} = \tilde{\phi}_{\alpha j}^{+,n} - \frac{\Delta t}{|V_j|}\boldsymbol{F}_{\alpha j}^{n+1/2}, \tag{22}$$

where

$$\tilde{\phi}_{\alpha j}^{+} = \frac{2\tau - \Delta t}{2\tau + \Delta t}\tilde{\phi}_{\alpha j} + \frac{2\Delta t}{2\tau + \Delta t}\phi_{\alpha j}^{eq}. \tag{23}$$

Note that the discrete scattering operator conserves energy, i.e, $\sum w_\alpha Q_\alpha = 0$, Therefore, we can track the evolution of $\tilde{\phi}_\alpha$ instead of ϕ_α, and from the definition of $\tilde{\phi}_\alpha$, the energy and heat flux can be computed as

$$E = \sum_{\alpha=1}^{N} w_\alpha \tilde{\phi}_\alpha, \quad \boldsymbol{q} = \frac{2\tau}{2\tau + \Delta t}\tilde{\boldsymbol{q}}, \quad \text{with} \quad \tilde{\boldsymbol{q}} = \sum_{\alpha=1}^{N} w_\alpha \boldsymbol{v}_\alpha \tilde{\phi}_\alpha, \tag{24}$$

where we have made use the fact that $\sum w_\alpha \boldsymbol{v}_\alpha \phi_\alpha^{eq} = \int_{4\pi} \boldsymbol{v}\phi^{eq}\, d\Omega = 0$.

3.2. Flux evaluation based on discrete characteristic solution

Now we discuss how to evaluate the cell interface flux at the half time-step, $\boldsymbol{F}_{\alpha j}^{n+1/2}$. To this end, we integrate Eq. (15) from t_n to $t_n + h$ (here $h = \Delta t/2$ is the half time step) along the characteristic line with the end point ($\boldsymbol{x}_b$) locating at the center of the cell interface (see Fig. 1),

$$\phi_\alpha(\boldsymbol{x}_b, t_n + h) - \phi_\alpha(\boldsymbol{x}_b - \boldsymbol{v}_\alpha h, t_n) = \frac{h}{2}[Q_\alpha(\boldsymbol{x}_b, t_n + h) + Q_\alpha(\boldsymbol{x}_b - \boldsymbol{v}_\alpha h, t_n)], \tag{25}$$

where the trapezoidal rule is again used to evaluate the scattering term. The implicitness in this equation can be removed by introducing another auxiliary distribution function $\bar{\phi}_\alpha$,

$$\bar{\phi}_\alpha = \phi_\alpha - \frac{h}{2} Q_\alpha = \frac{2\tau + h}{2\tau}\phi_\alpha - \frac{h}{2\tau}\phi_\alpha^{eq}, \tag{26}$$

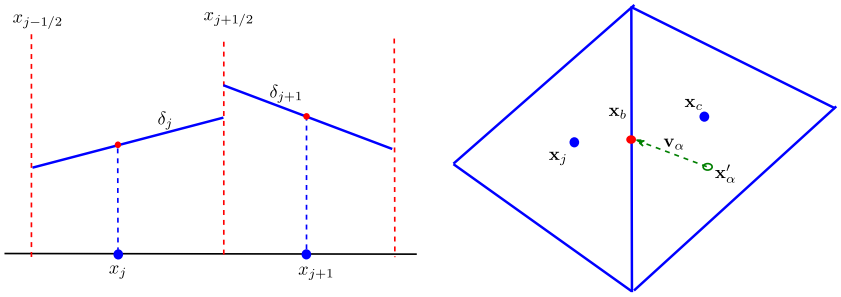

Fig. 1. Schematic of a 1D (a) and 2D (b) cell geometry.

or

$$\phi_\alpha = \frac{2\tau}{2\tau+h}\bar{\phi}_\alpha + \frac{h}{2\tau+h}\phi_\alpha^{eq}. \tag{27}$$

Then we can obtain from Eq. (25) that

$$\bar{\phi}_\alpha(\boldsymbol{x}_b, t_n+h) = \bar{\phi}_\alpha^+(\boldsymbol{x}_b - \boldsymbol{v}_\alpha h, t_n), \tag{28}$$

with

$$\bar{\phi}_\alpha^+ = \frac{2\tau-h}{2\tau}\phi_\alpha + \frac{h}{2\tau}\phi_\alpha^{eq}. \tag{29}$$

In order to determine $\bar{\phi}_\alpha^+(\boldsymbol{x}_b - \boldsymbol{v}_\alpha h, \boldsymbol{s}_\alpha, t_n)$, we assume that the distribution function is a piecewise linear function in the cell at which $\boldsymbol{x}'_\alpha = \boldsymbol{x}_b - \boldsymbol{v}_\alpha h$ locates, say the cell centered at $\boldsymbol{x}_c$ (refer to Fig. 1). Then we can obtain that

$$\bar{\phi}_\alpha^+(\boldsymbol{x}', t_n) = \bar{\phi}_\alpha^+(\boldsymbol{x}_c, t_n) - (\boldsymbol{x}'_\alpha - \boldsymbol{x}_c)\cdot\boldsymbol{\delta}_c\bar{\phi}_\alpha^{+,n}, \tag{30}$$

where $\boldsymbol{\delta}_c\bar{\phi}_\alpha^+$ is the slope of the distribution function $\bar{\phi}_\alpha^+$ in the cell centered at $\boldsymbol{x}_c$, which can be constructed smoothly or using certain numerical limiters. For instance, in 1D case as sketched in Fig. 1, the slope in cell j can be determined by the central-difference,

$$\delta_j\bar{\phi}_{\alpha j}^+ = \frac{x_{j+1}-x_j}{x_{j+1}-x_{j-1}}s_1 + \frac{x_j-x_{j-1}}{x_{j+1}-x_{j-1}}s_2, \tag{31}$$

for smooth problems, or by the van Leer limiter [31],

$$\delta_j\bar{\phi}_{\alpha j}^+ = [\mathrm{sgn}(s_1)+\mathrm{sgn}(s_2)]\frac{|s_1||s_2|}{|s_1|+|s_2|}, \tag{32}$$

for problems with discontinuities, where

$$s_1 = \frac{\bar{\phi}_{\alpha,j}^+ - \bar{\phi}_{\alpha,j-1}^+}{x_j - x_{j-1}}, \quad s_2 = \frac{\bar{\phi}_{\alpha,j+1}^+ - \bar{\phi}_{\alpha,j}^+}{x_{j+1}-x_j}. \tag{33}$$

It can be seen that in smooth region where $s_1 \approx s_2$, the slopes determined by the two methods are similar. For multi-dimensional case, the slope in each direction can be determined as described above.

Based on Eqs. (28) and (30), we can obtain that

$$\bar{\phi}_\alpha(\boldsymbol{x}_b, t_n+h) = \bar{\phi}_\alpha^+(\boldsymbol{x}_c, t_n) - (\boldsymbol{x}'_\alpha - \boldsymbol{c}_c)\cdot\boldsymbol{\delta}_c\bar{\phi}_\alpha^{+,n}, \tag{34}$$

from which we can obtain the energy at the cell interface,

$$E(\boldsymbol{x}_b, t_n+h) = \sum_\alpha \bar{\phi}_\alpha(\boldsymbol{x}_b, t_n+h), \tag{35}$$

where we have again used the energy conservative property of the discrete scattering operator. Then the equilibrium distribution function $\phi_\alpha^{eq}(\boldsymbol{x}_b, t_n+h)$ can be obtained, and the original distribution function can be extracted from $\bar{\phi}_\alpha(\boldsymbol{x}_b, t_n+h)$ according to Eq. (27),

$$\phi_\alpha(\boldsymbol{x}_b, t_n+h) = \frac{2\tau}{2\tau+h}\bar{\phi}_\alpha(\boldsymbol{x}_b, t_n+h) + \frac{h}{2\tau+h}\phi_\alpha^{eq}(\boldsymbol{x}_b, t_n+h). \tag{36}$$

With the known distribution function ϕ_α at cell interface at the half time step, the flux $\boldsymbol{F}_{\alpha j}^{n+1/2}$ can be evaluated according to Eq. (18), and the cell-averaged distribution functions $\tilde{\phi}_\alpha$ at the new time t_{n+1} can be obtained according to Eq. (22).

3.3. Algorithm

Summarizing the updating rule for the cell-averaged distribution functions and the interface flux, the DUGKS consists of the following two equations,

$$\tilde{\phi}_{\alpha j}^{n+1} = \tilde{\phi}_{\alpha j}^{+,n} - \frac{\Delta t}{|V_j|}\sum_{\boldsymbol{x}_b\in\mathcal{N}_j}\boldsymbol{v}_\alpha\phi_\alpha^{n+1/2}(\boldsymbol{x}_b), \tag{37}$$

$$\phi_\alpha^{n+1/2}(\boldsymbol{x}_b) = \frac{2\tau}{2\tau+\Delta t/2}\left[\bar{\phi}_\alpha^{+,n}(\boldsymbol{x}_c) + (\boldsymbol{x}'_\alpha - \boldsymbol{x}_c)\cdot\boldsymbol{\delta}_c\bar{\phi}_\alpha^{+,n}\right] + \frac{\Delta t/2}{2\tau+\Delta t/2}\phi_\alpha^{eq,n+1/2}(\boldsymbol{x}_b), \tag{38}$$

where

$$\tilde{\phi}_{\alpha j}^{+,n} = \tilde{\phi}_{\alpha j}^n + \frac{2\Delta t}{2\tau+\Delta t}\left[\phi_{\alpha j}^{eq,n} - \tilde{\phi}_{\alpha j}^n\right], \tag{39}$$

$$\bar{\phi}_{\alpha j}^{+,n} = \tilde{\phi}_{\alpha j}^n + \frac{3\Delta t/2}{2\tau+\Delta t}\left[\phi_{\alpha j}^{eq,n} - \tilde{\phi}_{\alpha j}^n\right]. \tag{40}$$

Note that we have made use of Eqs. (20) and (29) in the derivation of Eq. (40). In practical computations, $\tilde{\phi}_\alpha^+$ can be calculated from $\bar{\phi}_\alpha^+$,

$$\tilde{\phi}_\alpha^+ = \frac{4}{3}\bar{\phi}_\alpha^+ - \frac{1}{3}\tilde{\phi}_\alpha. \tag{41}$$

The calculation procedure of the DUGKS at time step t_n can be listed as follows:

(i) Flux evaluation:
- Compute the auxiliary distribution functions $\bar{\phi}_{\alpha j}^{+,n}$ according to Eq. (40) and its slope in each cell;
- Compute the original cell interface distribution function $\phi_\alpha^{n+1/2}(\boldsymbol{x}_b)$ according to Eq. (38), where $\phi_\alpha^{eq,n+1/2}$ is evaluated based on $E^{n+1/2}$ given by Eq. (35).

(ii) Update of Cell-averaged distribution functions:
- Compute the auxiliary distribution functions $\tilde{\phi}_{\alpha j}^{+,n}$ according to Eq. (41);
- Update the distribution functions $\tilde{\phi}_{\alpha j}^{n+1}$ in all cells via Eq. (37).

4. Analysis of the DUGKS

4.1. Numerical diffusion

Artificial diffusion can significantly deteriorate the simulation accuracy of a numerical scheme for the BTE. We now analyze the numerical diffusion of the proposed DUGKS by analyzing the accuracy of the reconstructed cell-interface distribution functions. First it is noted that the exact solution of the BTE (15) at cell interface center $\boldsymbol{x}_b$ can be written as

$$\phi_{\alpha,e}^{n+1/2}(\boldsymbol{x}_b) = \phi_\alpha^n(\boldsymbol{x}_b - h\boldsymbol{v}_\alpha) + \int_0^h Q_\alpha(\boldsymbol{x}_b - (h-t')\boldsymbol{v}_\alpha, t^n + t'))\,dt'. \tag{42}$$

The first and second terms on the right hand side represents the free transport and scattering processes, respectively. In the DUGKS, the trapezoidal rule is used to approximate the integral of the scattering term, and the approximation error in this term is $O(h^3)$; For the first term on the right hand side, it is approximated by assuming the distribution function is a linear function in the cell, and the error is of order $O(\Delta x^2)$. Therefore, the overall accuracy of the reconstructed distribution function at a cell interface at half time step in DUGKS is $O(\Delta x^2) + O(\Delta t^3)$, and the numerical diffusion coming from the numerical flux,

$$\boldsymbol{F}(\boldsymbol{x}_b) = \frac{1}{\Delta t}\int_0^{\Delta t}\int_{4\pi}\boldsymbol{v}_g\phi(\boldsymbol{x}_b, t)d\Omega dt, \tag{43}$$

will be of the order $O(\Delta x^2) + O(\Delta t^2)$ since the mid-point quadrature rule is employed for the time integration.

Note that the scattering term in Eq. (42) itself is of order Δt, so if we neglect the scattering term totally (i.e. only the free flight process is considered), like the classical first-order upwind (Step) scheme, second-order upwind or central interpolation (diamond) scheme, the overall accuracy of the reconstructed distribution function will be $O(\Delta x^n)+O(\Delta t)$, where the number n depends on the employed interpolation rule. Therefore, although the use of high-order interpolations can reduce numerical diffusion from spatial discretization, it is no help to reduce numerical diffusion from the scattering integration, which is of order $O(\tau)$. On the other hand, it is known from Eq. (12) that the physical diffusion coefficient is proportional to the relaxation time τ. This suggests that in order to control the numerical diffusion to avoid false diffusion, it is required that $\Delta t \ll \tau$. For problems in near ballistic regime, this is not a problem since τ is relatively large. However, for diffusive and near diffusive problems, this becomes a rather severe limitation. Therefore, for those explicit BTE solvers that use direct interpolations, the small time step is required not only by the numerical stability condition, but also by the accuracy requirement. This also explains why some implicit BTE solvers could produce large false diffusions even the computation is stable. On the other hand, the numerical diffusion from the discretization of the scattering term in present DUGKS is of order $O(\Delta t^2)$, which can release greatly the restriction on time step by the accuracy requirement.

4.2. Asymptotic preserving property

The Asymptotic preserving (AP) property is important for a kinetic scheme in modeling multiscale transport. A kinetic scheme is AP given that [29,30] (i) the time step Δt is not limited by the relaxation time τ for any Knudsen number, and (ii) the scheme is consistent with the free transport kinetic equation as $\mathrm{Kn}\to\infty$, and consistent with the continuum equation as $\mathrm{Kn}\to 0$.

Regarding Point (i), as discussed in the above subsection, the restriction on the time step by accuracy requirement can be much released due to the coupling in the treatment of the scattering and transport processes. Furthermore, the implicitness in the treatment of the collision terms with the trapezoidal rule in both the evolution of the cell-center distribution function (Eq. (17)) and the reconstruction of the cell-interface distribution (Eq. (25)) suggests that the restriction on the time step by numerical stability due to the relaxation time τ can be removed, too. Therefore, the constraint on the time step of DUGKS due to the free flight process can be ensured by the Courant–Friedrichs–Lewy (CFL) condition,

$$\Delta t=\beta\frac{\Delta x_{min}}{v_g}, \tag{44}$$

where Δx_{min} is the minimum cell size and $0<\beta\leqslant 1$ is the CFL number.

To demonstrate Point (ii), we first rewrite Eq. (38) in terms of the original distribution function as

$$\begin{aligned}\phi_\alpha^{n+1/2}(\boldsymbol{x}_b)=&A(\tau,\Delta t)\left[\phi_\alpha^n(\boldsymbol{x}_c)+(\boldsymbol{x}'_\alpha-\boldsymbol{x}_c)\cdot\boldsymbol{\delta}_c\phi_\alpha^n\right]\\&+B(\tau,\Delta t)\left[\phi_\alpha^{eq,n}(\boldsymbol{x}_c)+(\boldsymbol{x}'_\alpha-\boldsymbol{x}_c)\cdot\boldsymbol{\delta}_c\phi_\alpha^{eq,n}\right]\\&+B(\tau,\Delta t)\phi_\alpha^{eq,n+1/2}(\boldsymbol{x}_b).\end{aligned} \tag{45}$$

where the two parameters A and B are

$$A(\tau,\Delta t)=\frac{4\tau-\Delta t}{4\tau+\Delta t},\quad B(\tau,\Delta t)=\frac{\Delta t}{4\tau+\Delta t}.$$

Note that in the DUGKS the discrete distribution functions are assumed to be piecewise linear in each cell, and therefore Eq. (45) can also be expressed as

$$\begin{aligned}\phi_\alpha^{n+1/2}(\boldsymbol{x}_b)=&A(\tau,\Delta t)\left[\phi_\alpha^{n,c}(\boldsymbol{x}_b)-\frac{\Delta t}{2}\boldsymbol{v}_\alpha\cdot\boldsymbol{\delta}_c\phi_\alpha^n\right]\\&+B(\tau,\Delta t)\left[\phi_\alpha^{eq,n}(\boldsymbol{x}_b)-\frac{\Delta t}{2}\boldsymbol{v}_\alpha\cdot\boldsymbol{\delta}_c\phi_\alpha^{eq,n}\right]\\&+B(\tau,\Delta t)\phi_\alpha^{eq,n+1/2}(\boldsymbol{x}_b),\end{aligned} \tag{46}$$

where $\phi_\alpha^{n,c}(\boldsymbol{x}_b)=\phi_\alpha^n(\boldsymbol{x}_c)+(\boldsymbol{x}_b-\boldsymbol{x}_c)\cdot\delta_c\phi_\alpha^n$ is the value of the distribution function at cell interface $\boldsymbol{x}_b$ determined from cell $\boldsymbol{x}_c$.

The AP property of the DUGKS depends on the parameters A and B. If we define the macroscopic diffusive length and time scales, l_0 and t_0, respectively, such that $\lambda_0/l_0=\epsilon\sim\mathrm{Kn}$ and $\tau_0/t_0=\epsilon^2$, the parameters A and B can the be expressed as

$$A(\tau,\Delta t)=\frac{4\epsilon^2\tau'-\Delta t'}{4\epsilon^2\tau'+\Delta t'},\quad B(\tau,\Delta t)=\frac{\Delta t'}{4\epsilon^2\tau'+\Delta t'}, \tag{47}$$

where $\tau'=\tau/\tau_0$ and $\Delta t'=\Delta t/t_0$ are the dimensionless relaxation time and time step, respectively. In the ballistic limit ($\epsilon\to\infty$), we can obtain that $A=1$ and $B=0$, and thus

$$\phi_\alpha(\boldsymbol{x}_b)=\phi_\alpha^{n,c}(\boldsymbol{x}_b)-\frac{\Delta t}{2}\boldsymbol{v}_\alpha\cdot\boldsymbol{\delta}_c\phi_\alpha^n=\phi_\alpha(\boldsymbol{x}_b-\boldsymbol{v}_\alpha\Delta t/2),$$

which is just a solution of the free transport kinetic equation. Specifically, in the 1D case as sketched in Fig. 1, the reconstructed interface distribution function is

$$\begin{aligned}\phi_{\alpha,j+1/2}^{n+1/2}=&\left[\phi_{\alpha,j+1/2}^{n,L}-\frac{1}{2}v_\alpha\Delta t\delta_j\phi_\alpha^n\right]H(v_\alpha)\\&+\left[\phi_{\alpha,j+1/2}^{n,R}-\frac{1}{2}v_\alpha\Delta t\delta_{j+1}\phi_\alpha^n\right]\overline{H}(v_\alpha)\end{aligned} \tag{48}$$

where $\phi_{j+1/2}^L$ and $\phi_{j+1/2}^R$ are the left and right values of the distribution functions at cell interface $j+1/2$, respectively, H is the Heaviside function, $H(x)=1$ if $x>0$, and 0 otherwise, while $\overline{H}=1-H$. Therefore, the DUGKS given by Eq. (37) can be expressed explicitly as (note that $\tilde{\phi}_\alpha=\tilde{\phi}_\alpha^+=\phi_\alpha$ in this limit)

$$\begin{aligned}&\frac{\phi_{\alpha,j}^{n+1}-\phi_{\alpha,j}^n}{\Delta t}+\frac{v_\alpha}{\Delta x_j}\Big\{H(v_\alpha)\left[\phi_{\alpha,j+1/2}^{n,L}-\phi_{\alpha,j-1/2}^{n,L}\right]\\&+\overline{H}(v_\alpha)\left[\phi_{\alpha,j+1/2}^{n,R}-\phi_{\alpha,j+1/2}^{n,R}\right]\Big\}-\frac{v_\alpha^2\Delta t}{2\Delta x_j}\Big\{H(v_\alpha)\left[\delta_j\phi_\alpha^n-\delta_{j-1}\phi_\alpha^n\right]\\&+\overline{H}(v_\alpha)\left[\delta_{j+1}\phi_\alpha^n-\delta_j\phi_\alpha^n\right]\Big\}=0,\end{aligned} \tag{49}$$

which is a consistent finite-volume scheme of Lax-Wendroff type for the kinetic equation without scattering. This result suggests that the DUGKS is AP in the ballistic limit.

Now we discuss the AP property of the DUGKS in the diffusive limit ($\epsilon\to 0$). Under this limit, the distribution function can be approximated as (see Appendix A),

$$\phi_\alpha=\phi_\alpha^{eq}-\tau\boldsymbol{v}_\alpha\cdot\nabla\phi\approx\phi_\alpha^{eq}-\tau\boldsymbol{v}_\alpha\cdot\boldsymbol{\delta}_c\phi. \tag{50}$$

Substituting this approximation into Eq. (46) we can obtain that

$$\begin{aligned}\phi_\alpha^{n+1/2}(\boldsymbol{x}_b)=&(1-B)\phi_\alpha^{eq,n,c}(\boldsymbol{x}_b)-\tau\boldsymbol{v}_\alpha\cdot\boldsymbol{\delta}_c\phi_\alpha^{eq,n,c}+B\phi_\alpha^{eq,n+1/2}(\boldsymbol{x}_b)\\&+O(\tau\Delta t)\\=&(1-B)\phi_\alpha^{eq,n}(\boldsymbol{x}_b)-\tau\boldsymbol{v}_\alpha\cdot\boldsymbol{\delta}\phi_\alpha^{eq,n}+B\phi_\alpha^{eq,n+1/2}(\boldsymbol{x}_b),\end{aligned} \tag{51}$$

where we have assumed that in diffusive limit the distribution function is smooth across cell interfaces, i.e., $\phi_\alpha^{eq,n,c}=\phi_\alpha^{eq,n}$ and $\boldsymbol{\delta}_c\phi=\boldsymbol{\delta}\phi$. On the other hand, based on the properties of the angular quadrature given by Eq. (14), we have

$$\sum_\alpha w_\alpha\boldsymbol{v}_\alpha\phi_\alpha^{eq}=\boldsymbol{0},\quad\sum_\alpha w_\alpha\boldsymbol{v}_\alpha\boldsymbol{v}_\alpha\phi_\alpha^{eq}=\frac{v_g^2}{3}E\boldsymbol{I}. \tag{52}$$

Therefore, the macroscopic flux across the cell interface $\boldsymbol{x}_b$ can be obtained,

$$\mathcal{F}(\boldsymbol{x}_b) = \sum_\alpha w_\alpha \boldsymbol{v}_\alpha \phi_\alpha^{n+1/2}(\boldsymbol{x}_b) = -\frac{1}{3}\tau v_g^2 \delta E^n(\boldsymbol{x}_b) = -\kappa \delta E^n(\boldsymbol{x}_b). \tag{53}$$

Then by taking the zeroth angular moment of Eq. (37) we can obtain that

$$\frac{E_j^{n+1} - E_j^n}{\Delta t} - \frac{1}{|V_j|}\sum_{\boldsymbol{x}_b \in \mathcal{N}_j} \kappa \delta E^n(\boldsymbol{x}_b) = 0. \tag{54}$$

Specifically, for the 1D case, the above equation becomes

$$\frac{E_j^{n+1} - E_j^n}{\Delta t} - \frac{1}{\Delta x_j}\kappa[\delta E_{j+1/2}^n - \delta E_{j-1/2}^n] = 0, \tag{55}$$

which is just an explicit solver for the diffusion Eq. (11), suggesting that the DUGKS is also AP in the diffusive limit.

5. Boundary conditions

Generally three types of boundary conditions are used to describe the interactions between phonons and material boundaries [32,33], namely, specular reflection, thermalization, and diffusive reflection. The specular reflection is similar to that in classical gas kinetic theory. It assumes that a phonon is just reflected back to the domain with a reflection angle equal and opposite to the incident one after it hits the surface, such that the phonon energy density for directions $\boldsymbol{s}_\alpha$ entering the domain is given by

$$\phi_\alpha = \phi_{\alpha'}, \quad \boldsymbol{s}_\alpha \cdot \boldsymbol{n} > 0, \tag{56}$$

where $\boldsymbol{s}_{\alpha'} = \boldsymbol{s}_\alpha - 2(\boldsymbol{s}_\alpha \cdot \boldsymbol{n})\boldsymbol{n}$, with $\boldsymbol{n}$ the outward unit normal vector to the wall pointing into the domain. Therefore, for the specular reflection, the phonon energy is conserved and there is no energy transfer across the boundary.

In thermalization boundary condition, a phonon is absorbed as it strikes the boundary, and a new phonon in thermal equilibrium with boundary temperature is emitted into the domain. Therefore, the reflected phonon can be expressed as

$$\phi_\alpha = \phi_\alpha^{eq}(T_s), \tag{57}$$

where T_s is the temperature at the surface. Since $\tilde{\phi}_\alpha$ and $\bar{\phi}_\alpha$ are linear combinations of ϕ_α and ϕ_α^{eq}, the thermalization boundary condition in the DUGKS can also be expressed as $\tilde{\phi}_\alpha = \tilde{\phi}_\alpha^{eq}(T_s)$ and $\bar{\phi}_\alpha = \bar{\phi}_\alpha^{eq}(T_s)$. It can be seen that the thermalization boundary condition for phonon transport is very similar to the Maxwell diffuse scattering in the classical gas kinetic theory, which assumes the distribution function of reflected particles follows a Maxwellian one with the wall temperature and velocity. It is obvious that thermalization boundary condition allows for energy transfer across the surface.

In the diffusive reflection boundary condition, which should not be confused with the Maxwell diffuse scattering in gas kinetic theory, the phonons hitting the surface are reflected with equal probability along all possible angles, namely,

$$f(\boldsymbol{s}) = -\frac{1}{\pi}\int_{\boldsymbol{s}'\cdot\boldsymbol{n}<0} (\boldsymbol{s}'\cdot\boldsymbol{n}) f(\boldsymbol{s}')\, d\Omega, \tag{58}$$

or in terms of the discrete phonon energy distribution function,

$$\phi_\alpha = -\frac{1}{\pi}\sum_{\boldsymbol{s}_\beta\cdot\boldsymbol{n}<0} w_\beta(\boldsymbol{s}_\beta\cdot\boldsymbol{n})\phi_\beta, \tag{59}$$

where we have made use of the fact that $\sum_{\boldsymbol{s}_\beta\cdot\boldsymbol{n}>0} w_\beta(\boldsymbol{s}_\beta\cdot\boldsymbol{n}) = \int_{\boldsymbol{s}\cdot\boldsymbol{n}>0}(\boldsymbol{s}\cdot\boldsymbol{n})d\Omega = \pi$. Since the phonons hitting the surface are all reflected back to the domain, the total energy in the diffusive reflection boundary condition is conserved and no heat transfer occurs across the boundary. This can also be generalized to realized heat flux boundary condition, i.e.,

$$\phi_\alpha = -\frac{1}{\pi}\left[-\frac{q_0}{v_g} + \sum_{\boldsymbol{s}_\beta\cdot\boldsymbol{n}<0} w_\beta(\boldsymbol{s}_\beta\cdot\boldsymbol{n})\phi_\beta\right], \tag{60}$$

where q_0 is the specified heat flux norm to the boundary. Since ϕ_α^{eq} is independent of angular direction, the boundary conditions of $\tilde{\phi}_\alpha$ and $\bar{\phi}_\alpha$ used in DUGKS can be specified similarly.

6. Numerical tests

In this section we will apply the DUGKS to several heat transfer problems with different Knudsen numbers to test its performance. In the simulations, the CFL number is fixed at 0.9 unless stated otherwise. The van Leer limiter is employed to determine the slope $\boldsymbol{\delta}_c\phi_{j,\alpha}^+$ in each cell for problems as described in Subsection 3.2. The local coordinate system used in the simulations is shown in Fig. 2, where $\theta \in [0,\pi]$ and $\phi \in [0, 2\pi]$ are the polar and azimuthal angles, respectively. For the angular discretization, the conventional S_N quadrature [34] is found to be not accurate enough for large Kn and serious "ray effect" can appear, which was also found in [35]. Therefore, we will use the Gauss–Legendre quadrature [36] to increase the discrete directions. Specifically, for 1D case where only x direction is involved, we will used the Gauss–Legendre quadrature to discrete the direction cosine μ into N_μ points in $[-1, 1]$, and for 2D case where (x, y) are involved, another Gauss–Legendre quadrature is employed to discretize the azimuthal angle φ into N_φ points in $[0, \pi]$. The weights and abscissas of the Gauss–Legendre quadrature can be computed using standard computer code [37].

6.1. Heat conduction across and along a film

First we consider the heat conduction across a dielectric film of thickness L. The temperatures of the two boundaries located at $x = 0$ and $x = L$ maintain at T_0 and T_L, respectively. The problem is 1D and the energy distribution function e'' depends on spacial variable x and angular variable $s_x = \mu = \cos\theta$ only, such that we can define a reduced distribution function $e''(x,\mu)$ by integrating $e''(\boldsymbol{s})$ with respect to φ,

$$e''(x,\mu) = \int_0^{2\pi} e''(x,\mu,\sin\theta\cos\varphi,\sin\theta\sin\varphi)\, d\varphi, \tag{61}$$

and the BTE for the phonon energy density at steady state becomes

$$\mu\frac{\partial e''}{\partial x} = -\frac{1}{\lambda}[e'' - e^{eq}], \tag{62}$$

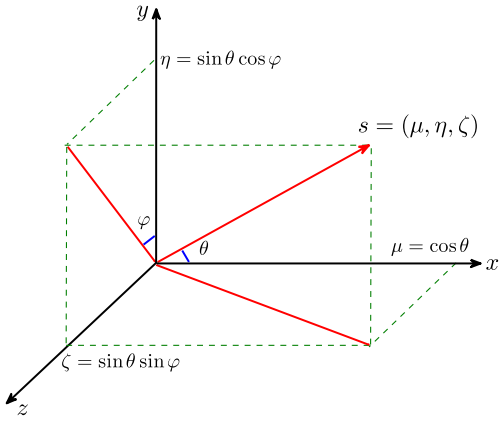

Fig. 2. Local coordinate system.

where $e^{eq}(x) = E(x)/2$ is the reduced equilibrium distribution for energy density. With the thermalizing boundary conditions at the two surfaces, the solution of this problem can be expressed as [3],

$$E^*(x^*) = \frac{1}{2}\left[E_2(x^*) + \int_0^{\xi} E^*(x')E_1(|x^* - x'|)\,dx'\right], \tag{63}$$

where $x^* = x/\lambda$ is the nondimensional position, $E^* = (E - E_0)/(E_L - E_0)$ is the nondimensional energy with $E_0 = C_V T_0$ and $E_L = C_V T_L$, $\xi = L/\lambda = 1/\mathrm{Kn}$ is the acoustic thickness, and $E_n(x) = \int_0^1 t^{n-2}\exp(-x/t)\,dt$ is the exponential integral function. The dimensionless heat flux $q^* = q/q_\infty$, with $q_\infty = v_g(E_0 - E_L)/4$ being the heat flux as $\mathrm{Kn} \to \infty$, can be expressed as

$$q^* = 1 - 2\int_0^{\xi} E^*(x')E_2(x')\,dx', \tag{64}$$

which is a constant across the domain. The two integration Eqs. (63) and (64) can be solved numerically to give an "numerical exact" solutions [3]. Here we use 4000 points such that the solutions are mesh independent.

The DUGKS is applied to this 1D problem at various Knudsen numbers, and in the simulations the Gauss–Legendre quadrature with $N_\mu = 100$ points is employed to evaluate the angular moments with respect to the directional cosine μ, i.e,

$$\begin{aligned} E(x) &= \int_{-1}^{1} e''(\boldsymbol{x},\mu)\,d\mu = \sum_{\alpha=1}^{N_\mu} w_\alpha \phi_\alpha(\boldsymbol{x}), \quad q(x) \\ &= \int_{-1}^{1} v_g \mu e''(\boldsymbol{x})\,d\mu = \sum_{\alpha=1}^{N_\mu} w_\alpha v_g \mu_\alpha \phi_\alpha(\boldsymbol{x}). \end{aligned} \tag{65}$$

It should be noted that here we choose $N_\mu = 100$ such that the moments can be evaluated accurately for all of the Knudsen numbers considered. Actually, a quadrature with much less angular points can be employed as $\mathrm{Kn} \leqslant 1$, say $N_\mu = 16$.

The dimensionless energy E^* and heat flux q^* with mesh resolutions of $N = 10$ and 200 are shown in Fig. 3. It can be observed that the DUGKS results agree well with the analytical solutions even with the coarse mesh, suggesting that the present scheme exhibits low numerical diffusion and is insensitive to mesh resolutions. The results also show the uniform stable property of the present DUGKS in the sense that the time step is solely determined by the CFL condition and is independent of the relaxation time. In other words, the time step Δt (or cell size Δx) is not required to be smaller than the relaxation time τ (or mean free path λ). Actually, with the coarse mesh ($N = 10$), the value of $\Delta x/\lambda = 1/(N\mathrm{Kn})$ ranges from 0.001 to 100 as Kn changes from 10^{-3} to 10^2, and $\Delta t/\tau$ ranges from 9×10^{-4} to 90.

For comparison, we also applied the implicit finite-difference method with step discretization of the convection term of Eq. (15), which is widely used for solving the phonon BTE [12,32,35] (see Appendix B for details), to the present problem. The profiles of the dimensionless energy E^* at various Kn are shown in Fig. 4. It can be observed with the fine mesh of $N = 200$, the results agree well with the analytical solutions as Kn changes from 0.01 to 10. This is reasonable since $\Delta x/\lambda \leqslant 0.5$ in all of the considered cases, and the numerical diffusion, which is proportional to Δx, is less than the physical one with this mesh resolution. On the other hand, with the coarse mesh, clear deviations from the analytical solutions can be observed as $\mathrm{Kn} = 0.01$ and 0.2.

We also applied the DUGKS method to study the heat conduction along a film. The configuration is similar to the above cross-plane case, but the two boundaries at $x = 0$ and $x = L$ are diffusive and maintain the same temperature in this case. A temperature gradient is imposed along the y-direction, namely, the top and bottom boundaries at $y = 0$ and $y = H$ maintain constant temperature T_0 and T_H, respectively. Unlike the across-plane case, this in-plane problem is two-dimensional, and the BTE at steady state can be expressed as [3],

$$\mu\frac{\partial e''}{\partial x} + \eta\frac{\partial e''}{\partial y} = -\frac{1}{\lambda}[e'' - e^{eq}]. \tag{66}$$

By introducing a deviation distribution function $g = e'' - e^{eq}$, the BTE can be approximated as [3]

$$\mu\frac{\partial g}{\partial x} + \eta\frac{\partial e^{eq}}{\partial T}\frac{\partial T}{\partial y} = \frac{g}{\lambda}. \tag{67}$$

Note that the second term on the left hand side can be approximated well from the constant temperature gradient, and so an approximation solution of g can be obtained,

$$g(x^*,\mu,\eta) = \begin{cases} \eta\frac{\partial e^{eq}}{\partial T}\frac{\partial T}{\partial y}\left[\exp\left(-\frac{x^*}{\mu}\right) - 1\right], & \mu > 0, \\ \eta\frac{\partial e^{eq}}{\partial T}\frac{\partial T}{\partial y}\left[\exp\left(\frac{\xi - x^*}{\mu}\right) - 1\right], & \mu < 0, \end{cases} \tag{68}$$

from which the in-plane effective thermal conductivity can be obtained [3] (the expression of heat flux is not available in the reference),

$$q_y(x^*) = \kappa_b \partial_y T\left\{1 - \frac{3}{4}[E_2(\xi - x^*) - E_4(\xi - x^*) + E_2(x^*) - E_4(x^*)]\right\}, \tag{69}$$

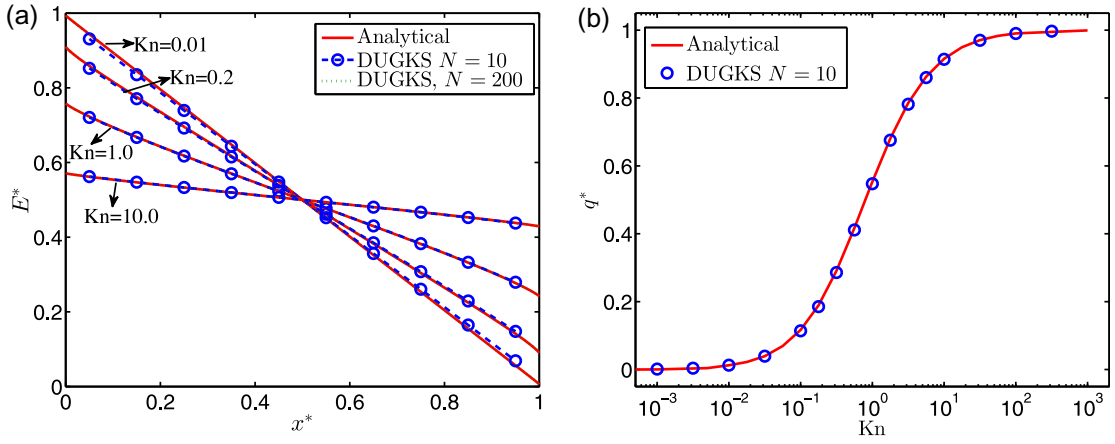

Fig. 3. Dimensionless energy and heat flux across a film.

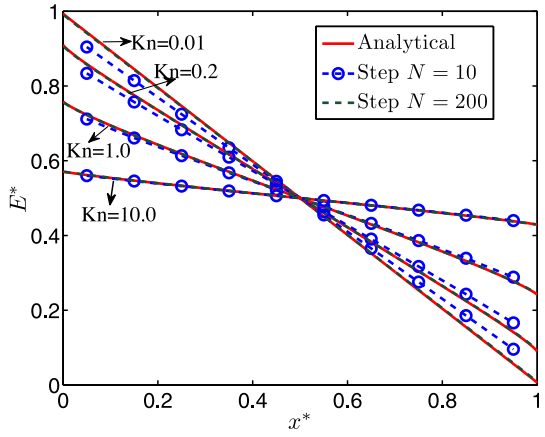

Fig. 4. Dimensionless energy from the step method across a film.

$$\kappa \equiv \frac{H}{T_0 - T_H}\frac{1}{L}\int_0^L q_y(x)\,dx = \kappa_b\left\{1 - \frac{3}{8\xi}[1 - 4E_3(\xi) + 4E_5(\xi)]\right\}. \quad (70)$$

where $\kappa_b = C_V \tau v_g^2/3$ is the thermal conductivity of bulk material.

The DUGKS method is applied to this in-plane heat conduction in a domain $0 \leqslant x \leqslant 1$ and $0 \leqslant y \leqslant 0.5$. The diffuse scattering boundary conditions are applied to the left and right boundaries, while the periodic boundary conditions developed in [38] are applied to the y-direction,

$$\phi_\alpha(x,0) = \phi_\alpha^{eq}(x,0) + \phi_\alpha(x,L) - \phi_\alpha^{eq}(x,L), \quad \mu_\alpha > 0 \quad (71a)$$

$$\phi_\alpha(x,L) = \phi_\alpha^{eq}(x,L) + \phi_\alpha(x,0) - \phi_\alpha^{eq}(x,0), \quad \mu_\alpha < 0 \quad (71b)$$

In the simulations, a uniform mesh of size $N_x \times N_y = 20 \times 10$ is used, and the angular space is discretized into $N_\mu \times N_\varphi = 100 \times 16$ directions to overcome the ray effect at large Knudsen numbers.

The profiles of the normalized heat flux $q_y^* = q_y/\kappa_b \partial_y T$ and the normalized thermal conductivity κ/κ_b are shown in Fig. 5. It can be seen that heat flux profiles predicted by the DUGKS agree excellent with the analytical solutions at the three Knudsen numbers even with this relative coarse mesh. The predicted thermal conductivity is also in excellent agreement with the analytical value from diffusive to ballistics regimes. It should be noted that in this test $\Delta x/\lambda$ and $\Delta t/\tau$ vary from order of 10^{-3} to 10^2. These results confirm the capability of the presented DUGKS in simulating heat transfer process at different Knudsen numbers.

6.2. Heat relaxation of transient thermal grating

The transient thermal grating (TTG) is a technique for measuring thermal conductivity and phonon mean free path of a material [39,40]. Here we considered the thermal relaxation process of a 1D TTG [40], where initially two crossed laser pulses are imposed to produce a spatially sinusoidal temperature variation in the medium,

$$T(x,0) = T_b + A_0 \cos(\theta x), \quad (72)$$

where T_b is the background temperature, A_0 is the amplitude of the temperature variation, and $\theta = 2\pi/l$ is the wave number with l being the grating period. As the strength of the pulse is weak, the BTE can be linearized, and the temperature deviation from the background temperature, $\Delta T = T - T_b$, can be approximated as $\Delta T(x,t) = A(t)\cos(\theta x)$, where the amplitude A can be obtained analytically [40],

$$\widehat{A}(t^*) = \mathrm{sinc}(\xi t^*)e^{-t^*} + \int_0^{t^*} \widehat{A}(t')\mathrm{sinc}[\xi(t'-t^*)]e^{(t'-t^*)}\,dt', \quad (73)$$

with $\widehat{A} = A/A_0$ and $t^* = t/\tau$, and $\xi = 2\pi\mathrm{Kn}$ is the rarefaction parameter with the Knudsen number defined as $\mathrm{Kn} = v_g\tau/l$. Eq. (73) is a second kind Volterra integral equation and can be solved using standard numerical techniques [41]. In the diffusive limit ($\xi \to 0$), it can be shown that

$$\widehat{A}(t^*) = e^{-\gamma t^*}, \quad (74)$$

where $\gamma = \xi^2/3$; while in the ballistic limit ($\xi \to \infty$), we have $\widehat{A}(t^*) = \mathrm{sinc}(\xi t^*)$, which shows strong oscillations.

We simulate the thermal relaxation process of the 1D TTG at different Knudsen numbers. The length of the computation domain is taken to be $L = 2l$, and a uniform grid of 100 points (i.e., 50 points in one grating period) is used for all cases. The directional cosine space $-1 \leqslant \mu \leqslant 1$ is discretized using the Gauss–Legendre quadrature with $N_\mu = 100$ points. Periodic boundary conditions are applied to the left ($x = 0$) and right ($x = L$) boundaries. In Fig. 6 the time histories of the amplitude of the temperature variation are shown for different values of ξ. It can be seen that the numerical results of the DUGKS are in excellent agreement with the analytical solutions for different Knudsen numbers, ranging from diffusive limit to ballistic limit. It is noted that the ratio of mesh size over the mean-free-path, $\Delta x/\lambda = 4\pi/\xi N$, spans from

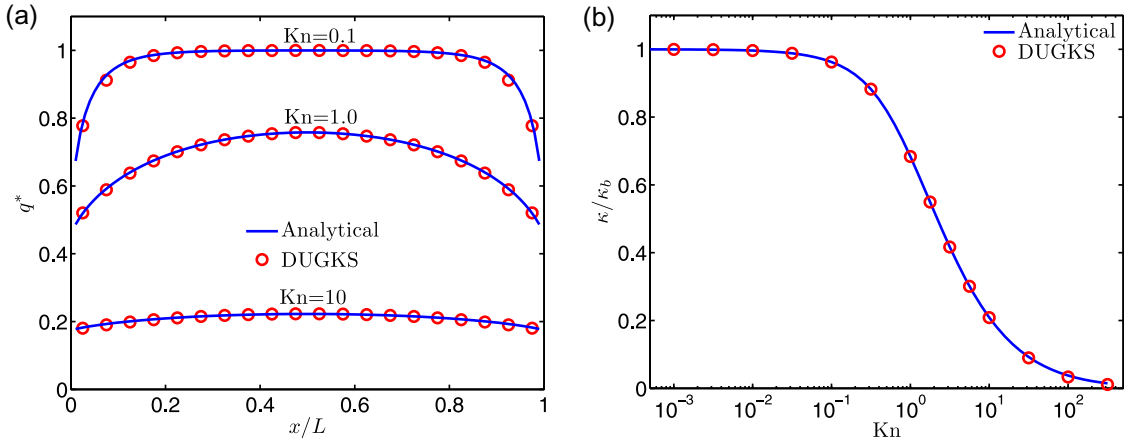

Fig. 5. Heat flux (a) and thermal conductivity of the in-plane heat transfer along a film.

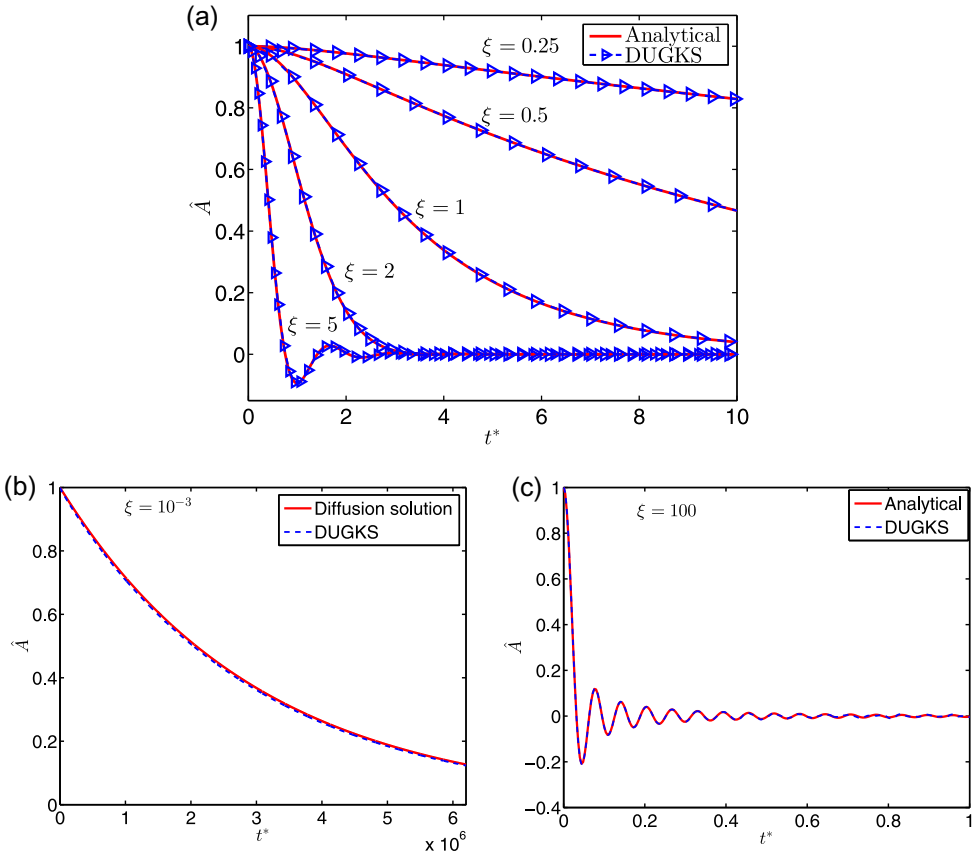

Fig. 6. Decaying of the dimensionless amplitude of temperature variation $\widehat{A} = A/A_0$ against dimensionless time $t^* = t/\tau$ at different Knudsen numbers $\xi = 2\pi\mathrm{Kn}$. (a) Finite values of ξ; (b) Diffusive limit; (c) Ballistic limit.

$4\pi \times 10^{-4}$ to 40π as ξ changes from 10^{-3} to 100 in this test, and the corresponding ratio of time step over relaxation time, $\Delta t/\tau$, spans from $3.6\pi \times 10^{-4}$ to 36π. The results again confirm the asymptotic preserving properties of the present DUGKS method.

6.3. Heat transfer in a 2D square domain

In the above subsections the DUGKS was tested by 1D steady and 1D unsteady heat transfer problems. We now consider a two-dimensional problem in a square medium of length L. Initially the temperature of the medium is set to be a uniform value T_0, and then the temperature at the bottom side ($y = 0$) is raised to and maintained at $T_1 > T_0$. Thermalization boundary conditions are assumed on the four sides, and the Knudsen number of the system is defined as $\mathrm{Kn} = \lambda/L$. This problem was studied recently by solving the BTE with a DOM coupled with finite-element scheme [13], and a similar radiative heat transfer was studied early [42], which is actually identical to the phonon transfer as the medium is exposed to isotropically scattering.

Simulations at different Knudsen numbers are conducted based on a uniform mesh $N_x \times N_y = 40 \times 40$ in physical space, and the directional cosine $\mu \in [-1, 1]$ (i.e., $0 \leqslant \theta \leqslant \pi$) is discretized with the 32-point Gauss–Legendre quadrature, while the azimuthal angular space $\varphi \in [0, \pi]$ (not $[0, 2\pi]$ due to symmetry) is discretized with the 16-point Gauss–Legendre quadrature. The CFL number is set to be 0.5 in this case. Our simulations show that the meshes are sufficient to obtain convergent results.

In Fig. 7 the normalized temperatures, $\Theta = (T - T_0)/(T_1 - T_0)$, are shown along the vertical centerline at $x = L/2$ as the system reaches the steady state. For comparison, we also present the solutions of DOM for phonon BTE [13] and the numerical analytical solutions of the integral equation describing radiative transfer in a 2D isotropically scattering medium [42]. It can be seen that the results of the DUGKS agree quite well with the reference data for all Knudsen numbers considered here. It is noted that some slight oscillations appear in the temperature profile predicted by the DOM at $\mathrm{Kn} = 10$ [13]. This is caused by the ray effect due to the insufficient discretization in angular space, which was based on a $N_\mu \times N_\varphi = 32 \times 8$ Gaussian quadrature [13]. On the other hand, the temperature profile from the present DUGKS does not show this behavior with the 32×16 angular discretization.

The transient behavior of this 2D problem is also compared with the results of Fourier solution at $\mathrm{Kn} = 0.01$ and DOM at

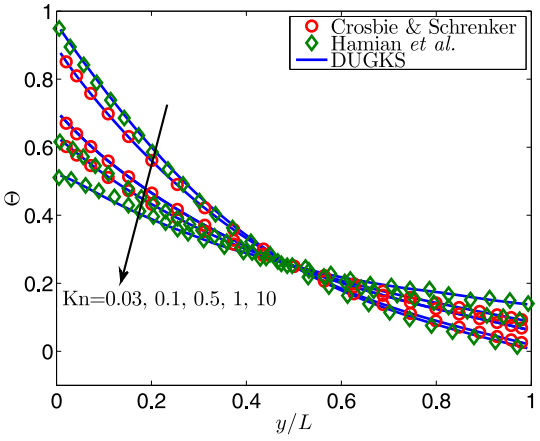

Fig. 7. Normalized temperature profile along the vertical centerline at different Knudsen numbers. Reference data are taken from Refs. [13,42].

Kn = 0.1, 1, and 10 [13]. The temperature profiles along the vertical centerline of the medium are shown in Fig. 8 at different times of $t^* = t/\tau$ for different Knudsen numbers ranging from diffusive to ballistic regimes. It can be observed that the DUGKS results agree qualitatively well with the benchmark data from initial to later times in all cases considered. Specifically, as Kn = 0.01, the heat transfer is diffusive, and no obvious temperature jump occurs at the top and bottom boundaries at different times. As Kn increases to 0.1, i.e., the problem falls in the near diffusive regime, and temperature jump appears on both boundaries, particularly on the bottom hot surface, where the jump decreases with time. At Kn = 1, temperature jump is more significant, but transient jump becomes smaller than that for the case of Kn = 0.1. As Kn = 10, the heat transfer is dominated by ballistic effect, and the temperature jump maintains nearly constant on the hot surface, although transient changes can still be observed on the bottom cold surface. It is also noted that some differences between the present results and the DOM data for the case of Kn = 10 at $t^* = 0.07$, which can again be attributed to the insufficient angular discretization of the DOM.

The transient heat flux in the y-direction along the vertical centerline of the domain are shown in Fig. 9, where the normalized heat flux is defined as $q_y^* = q_y/q_F$, with q_F being the steady heat flux at the middle point of the hot boundary ($y = 0$) from the solution of the Fourier conduction equation [13]. At Kn = 0.01, it can be seen at the early stage ($t^* = 1.0$), the heat flux of the DUGKS solution is smaller than the transient Fourier solution. Such discrepancy was also observed in Ref. [13], and was attributed to the difference between the BTE and Fourier model, where the contribution of ballistic phonon transport in the early transient behavior is important. At the later stage ($t^* = 10^3$ and 10^4), diffusive transport dominates the heat transfer and the heat flux predicted by the DUGKS agree well with the Fourier solutions. For the cases of Kn = 0.1, 1, and 10, the profiles of the normalized heat flux agree well with the DOM solutions. The above results of this 2D heat transfer problem confirm the AP and uniform stable properties of the proposed DUGKS for simulating heat transport process from diffusive to ballistic regimes.

It is noted that in this test case, the mesh size and time step are again not required to be smaller than the mean-free path and relaxation time, respectively. Actually, $\Delta x/\lambda$ and $\Delta t/\tau$ change from 2.5×10^{-3} to 2.5 and 1.25×10^{-3} to 1.25 for $0.01 \leqslant \mathrm{Kn} \leqslant 10$, respectively.

6.4. Multiscale heat transfer across an inhomogeneous film

To further test the capability of the present DUGKS method in simulating multiscale heat transfer problems, we now apply it to a film of thickness L with inhomogeneous acoustic property. The configuration is the same as the problem considered in Subsection 6.1, except that the relaxation time varies across the film,

$$\tau(x) = \frac{\tau_{max} + \tau_{min}}{2} - \frac{\tau_{max} - \tau_{min}}{2} \tanh\left(\frac{x - x_0}{2d}\right), \tag{75}$$

where τ_{min} and τ_{max} are the minimum and maximum values of the relaxation time, respectively, $x_0 = L/2$ is the center of the film, and d is a small parameter characterizing the thickness of the transition layer. This configuration models a film composed of two materials with a diffusive interface, the acoustic thicknesses of which, $0.5L/(v_g\tau_{min})$ and $0.5L/(v_g\tau_{max})$, can differ significantly. The Knudsen number of the system changes between $\mathrm{Kn}_{min} = v_g\tau_{min}/L$ and $\mathrm{Kn}_{max} = v_g\tau_{max}/L$.

Simulations of the above problem are carried out to test the capability of the present DUGKS method for simulating multiscale heat transfer process. We choose $L = 1.0, v_g = 1.0, d = 0.01$,

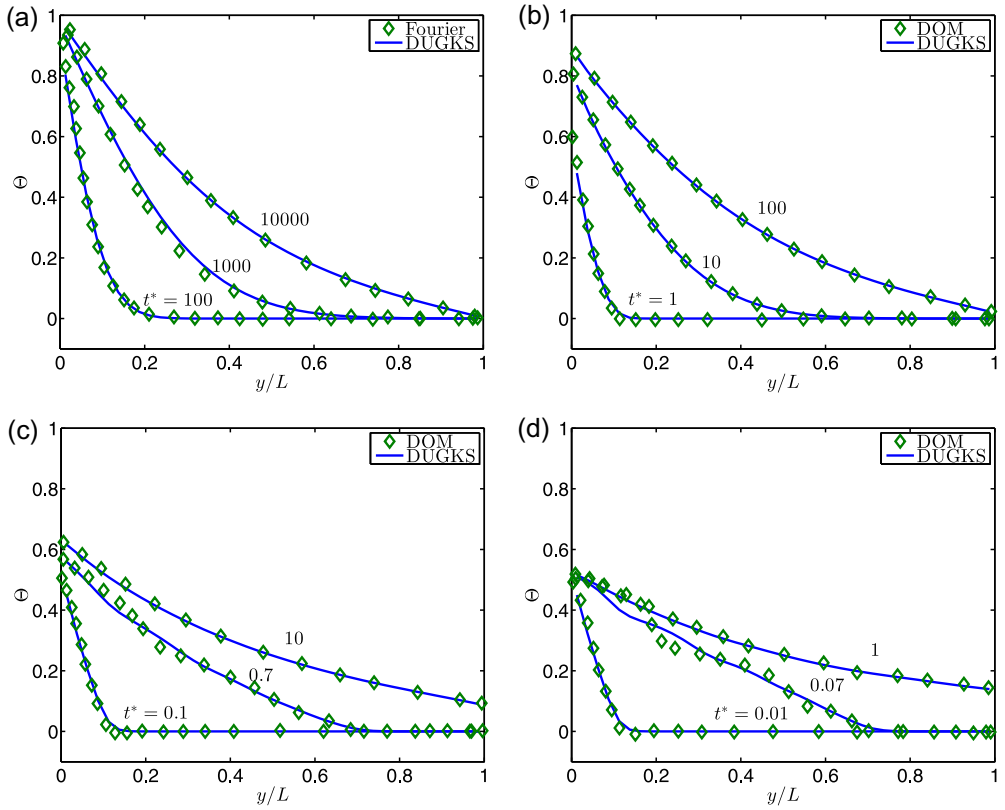

Fig. 8. Transient temperature profile along the vertical centerline at different Knudsen numbers. (a) Kn = 0.01, (b) Kn = 0.1, (c) Kn = 1.0, and (d) Kn = 10.0, The Fourier and DOM data are taken from Ref. [13], and $t^* = t/\tau$.

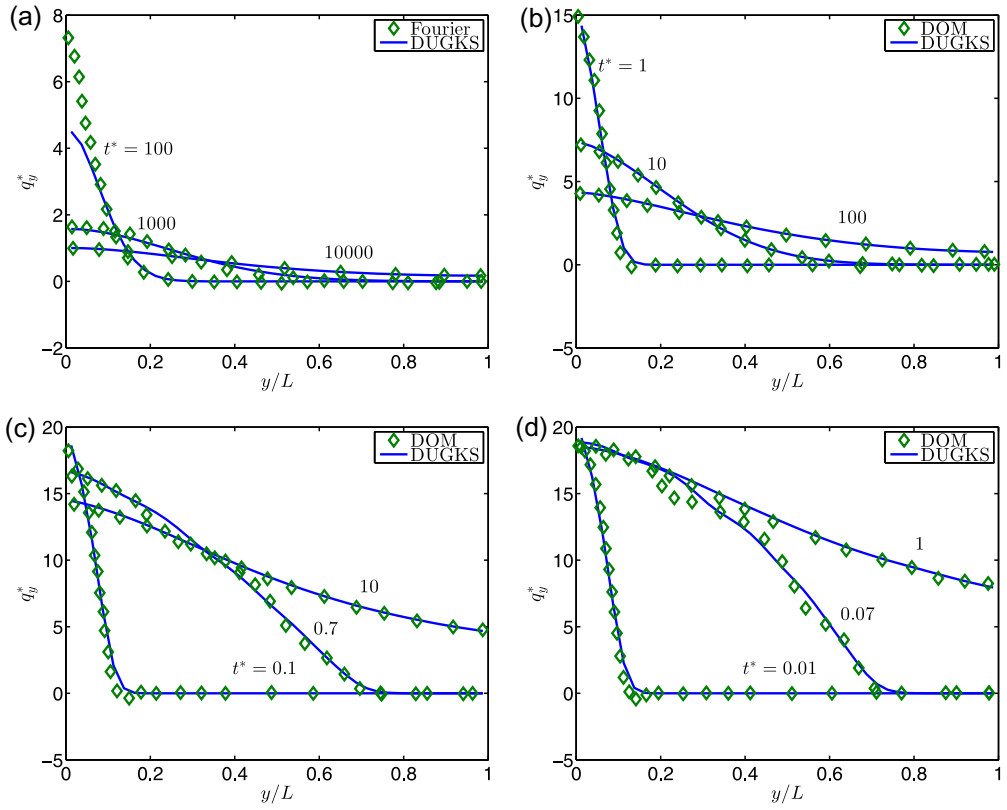

Fig. 9. Transient heat flux along the vertical centerline at different Knudsen numbers. (a) Kn = 0.01, (b) Kn = 0.1, (c) Kn = 1.0, and (d) Kn = 10.0, The Fourier and DOM data are taken from Ref. [13].

$\tau_{min} = 10^{-4}$, and $\tau_{max} = 10.0$, such that $\mathrm{Kn}_{min} = 10^{-4}$ and $\mathrm{Kn}_{max} = 10$, and therefore the heat transfer process across the film is a multiscale problem. The profile of the relaxation time is shown in Fig. 10. It can be seen that τ changes smoothly across the interfacial region $0.45 < x < 0.55$, and maintains nearly the constant values (τ_{min} and τ_{max}) in the bulk regions. The heat transfer is dominated by diffusive conduction and ballistic transport in the regions $0 \leqslant x \leqslant 0.45$ and $0.55 \leqslant x \leqslant 1$, respectively, and transitional transport occurs in the interfacial region. The large span of Knudsen number as well as the large gradient in the interfacial region can bring difficulties for numerical simulations, and therefore this problem can serve as a good test case for the present multiscale numerical scheme.

In the simulations, the temperature over across the whole domain is initialized as $T(x,0) = (T_0 + T_L)/2$, where T_0 and T_L are the fixed temperatures at the left ($x = 0$) and right ($x = L$) boundaries, respectively. A uniform mesh of size $N = 80$ is employed, and the CFL number (β) is set to be 0.8 such that $\Delta x/\lambda$ and $\Delta t/\tau$ change from 0.00125 to 125 and 0.001 to 100, respectively.

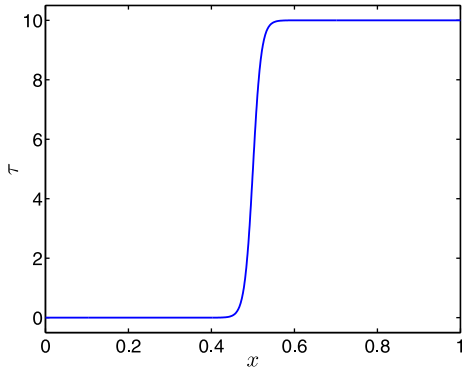

Fig. 10. The distribution of relaxation time given by Eq. (75) with $\tau_{min} = 10^{-4}, \tau_{max} = 10, x_0 = 0.5, d = 0.01$.

For this problem no analytical solution is available, and grid-independent reference solutions at different times are obtained by an explicit second-order upwind (denoted by 2nd-Upwind) scheme (see Appendix B) with a uniform mesh of $N = 10,000$ cells and a time step $\Delta t = 0.1\Delta x/v_g = 10^{-5}$. Fig. 11 shows the profiles of the normalized temperature, $\Theta = (T - T_0)/(T_L - T_0)$, at $t^* = t/(L/v_g) = 1$, 10, 20, and 50. The results of the Step and 2nd-Upwind methods are also shown for comparisons. Here the CFL number β is set to be 0.8 for the Step scheme, and 0.01 for the 2nd-Upwind scheme because the computation blows up as $\beta \geqslant 0.02$. From Fig. 11 we can observe that the results of the DUGKS agree excellent with the reference solutions at all of the four times. On the other hand, the Step method over-predicts the temperature at the ballistic region, while the 2nd-Upwind method shows significant deviations in the diffusive region.

The profiles of heat flux normalized by the ballistic value, $q^* = q/q_\infty$, are also compared at the four times (Fig. 12). It can be observed that the Step method gives significant over-predictions in the ballistic region at late stages ($t^* \geqslant 10.0$), although the deviations at the early state ($t^* = 1$) is relatively small. On the other hand, the results of the DUGKS show excellent agreement with the reference solutions over the whole region at all stages. The second-order upwind method yields better results than the Step method since the false diffusion is much smaller than the latter. However, the deviations from the reference solutions are still obvious in both diffusive and ballistic regions. The above results clearly show the robust property of the DUGKS for multiscale heat transfer problems.

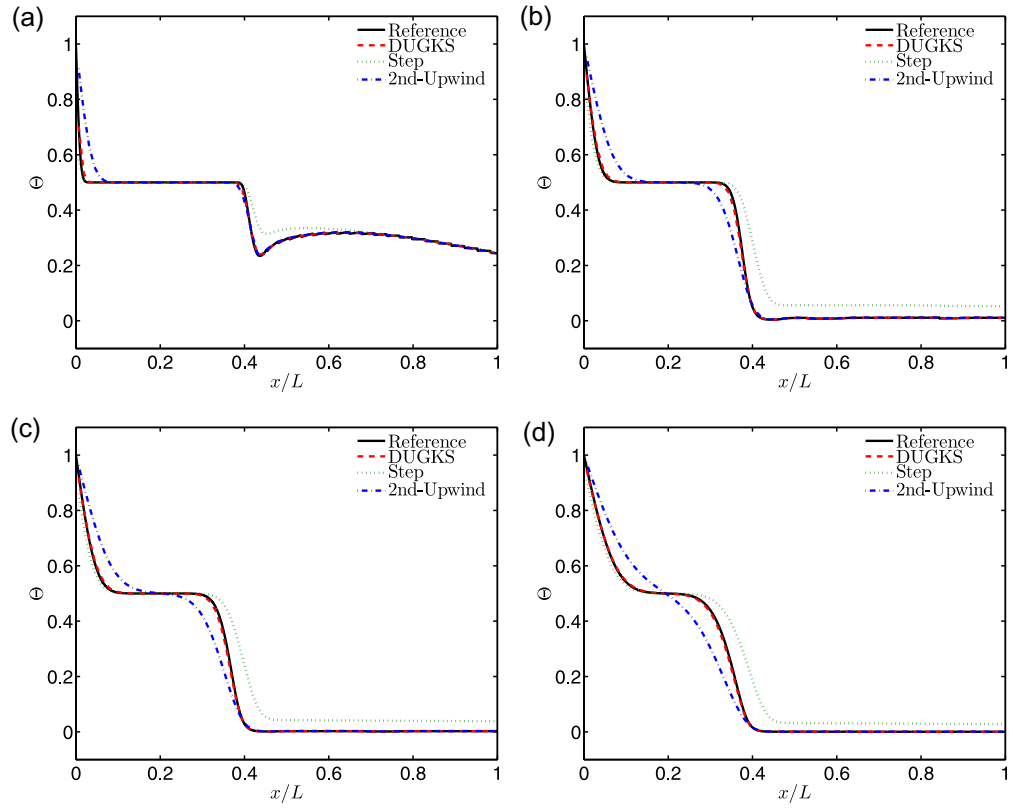

Fig. 11. Nondimensional temperature at different times. (a) $t^* = 1.0$, (b) $t^* = 10$, (c) $t^* = 20$, and (d) $t^* = 50$. Here $t^* = t/(L/v_g)$.

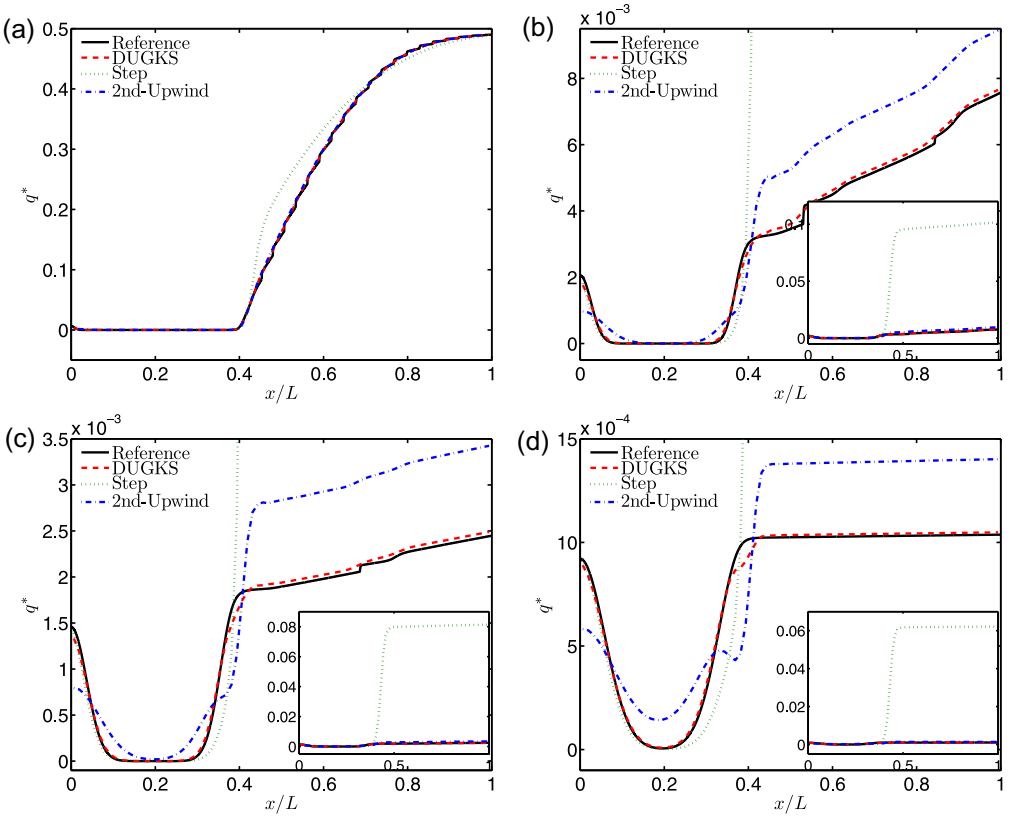

Fig. 12. Same as Fig. 11 but for the nondimensional heat flux. Inset: global view of the heat flux profile.

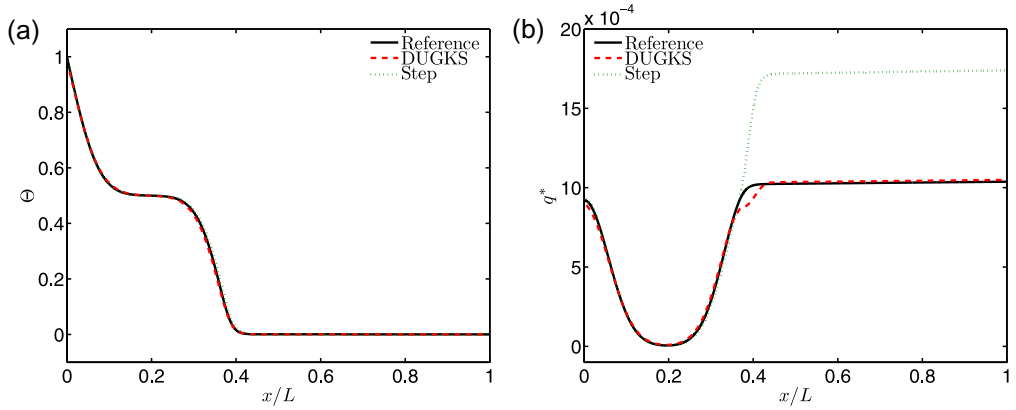

Fig. 13. The nondimensional temperature and heat flux for the Step ($N = 10^4$) and DUGKS ($N = 80$) at $t^* = 50$. The CFL number is 0.8 for both methods.

The computational time for each method is also measured. It is found with the same mesh ($N = 80$) and CFL number ($\beta = 0.8$), the DUGKS and Step methods take about 0.79 and 1.03 seconds to march to $t^* = 50$, respectively. But the 2nd-Upwind method takes about 47.88 seconds with the small CFL number ($\beta = 0.01$), which is much expensive than the DUGKS and Step methods. Although the computational cost of the Step method is comparable to the DUGKS with the same mesh size and time step, its prediction is much poorer, as shown above. Actually, we found the mesh size is required to increase to $N = 10^4$ at least for the Step scheme to obtain results comparable to DUGKS (see Fig. 13 as an example). However, with this finer mesh, the Step scheme takes around 10.6 hours to reach to $t^* = 50$. The above results clearly demonstrate that the present DUGKS is an efficient method for multiscale heat transfer problems.

7. Summary

In this work we develop a discrete unified gas kinetic scheme for multiscale heat transfer based on the phonon Boltzmann transport equation. With the coupled treatment of the scattering and transport of phonons, the scheme is asymptotic preserving, and the limitation on the time step being less than the relaxation time in diffusive regime is removed. The method has been validated by the 1D in-plane and across-plane heat conduction problems, a transient 1D TTG problem, a 2D problem at different Knudsen numbers, and a multiscale heat transfer across an inhomogeneous film. The results are in excellent agreement with analytical or reference data.

In the present work, the proposed DUGKS is designed based on the gray BTE model, where the frequency dependence of the distribution function, relaxation time, and group velocity, are ignored. Different phonon polarizations are indistinguishable in the gray model, and energy exchange between different modes cannot be clearly identified. Therefore, for systems where the phonon relaxation mechanisms are important non-gray models should be employed [1]. The current methodology can be extended to non-gray BTE models by discretizing the frequency domain into finite groups. We will consider non-gray problems in our subsequent studies.

Acknowledgments

ZLG acknowledges the support by the National Natural Science Foundation of China (51125024), and part of the work was carried out during his visit to the Hong Kong University of Science and Technology. The research of KX was supported by Hong Kong Research Grant Council (620813, 16211014, 16207715) and HKUST research fund (PROVOST13SC01, IRS15SC29, SBI14SC11).

Appendix A. Analysis of the BTE with diffusive scaling

In order to analyze the limiting behavior of the BTE in the diffusive regime, we here make use of the diffusive scaling analysis introduced by Sone in gas kinetic theory [43], which was also used in the analysis of the Unified Gas Kinetic Scheme for radiative transper problems [44]. With the diffusive scaling, i.e., $t_0 = t/\epsilon^2$ and $x_0 = x/\epsilon$ with $\epsilon \sim \mathrm{Kn}$ being a small parameter, we have

$$\partial_t = \epsilon^2 \partial_{t_0}, \quad \partial_{x_i} = \epsilon \partial_{x_0}. \tag{A.1}$$

Then the BTE (7) can be rewritten as

$$\epsilon^2 \partial_{t_0} e'' + \epsilon \boldsymbol{v}_\alpha \cdot \nabla_0 e'' = -\frac{1}{\tau}[e'' - e^{eq}]. \tag{A.2}$$

We further expand e'' in a power series of ϵ,

$$e'' = e^{(0)} + \epsilon e^{(1)} + \epsilon^2 e^{(2)} + \cdots. \tag{A.3}$$

Substituting this expansion into Eq. (A.2), we can obtain the equations in the consecutive orders of ϵ,

$$\epsilon^0: \quad e^{(0)} = e^{eq}, \tag{A.4a}$$

$$\epsilon^1: \quad \boldsymbol{v} \cdot \nabla_0 e^{(0)} = -\frac{1}{\tau} e^{(1)}, \tag{A.4b}$$

$$\epsilon^2: \quad \partial_{t_0} e^{(0)} + \boldsymbol{v} \cdot \nabla_0 e^{(1)} = -\frac{1}{\tau} e^{(2)}. \tag{A.4c}$$

From Eqs. (A.3) and (A.4a), and recalling the energy conservative property of the scattering operator, we have that

$$\int_{4\pi} e^{(k)}\, d\Omega = 0, \quad k \geqslant 1. \tag{A.5}$$

Then taking moment of Eq. (A.4c) we can obtain the following macroscopic equation,

$$\partial_{t_0} E + \nabla_0 \cdot \boldsymbol{q}^{(1)} = 0, \tag{A.6}$$

where $\boldsymbol{q}^{(1)} = \int_{4\pi} \boldsymbol{v} e^{(1)}\, d\Omega$, which can be obtained from Eq. (A.4b) as

$$\begin{aligned} \boldsymbol{q}^{(1)} &= -\tau \nabla_0 \cdot \int_{4\pi} \boldsymbol{v}\boldsymbol{v} e^{(0)}\, d\Omega = -v_g^2 \tau \nabla_0 \cdot \int_{4\pi} \boldsymbol{s}\boldsymbol{s} e^{(0)}\, d\Omega \\ &= -\frac{v_g^2 \tau}{3} \nabla_0 E, \end{aligned} \tag{A.7}$$

which is exactly the Fourier law. Therefore, the heat transfer equation at the (macroscopic) diffusive length and time scales are

$$\partial_{t_0} E - \nabla_0 \cdot (\kappa \nabla_0 E) = 0, \tag{A.8}$$

or

$$\partial_t E - \nabla \cdot (\kappa \nabla T) = 0, \tag{A.9}$$

with $\kappa = C_V v_g^2 \tau/3$ being the heat conductivity.

With the equations at different orders of ϵ given by Eq. (A.4), we can obtain an approximation of the energy distribution function at the first order of ϵ,

$$e'' \approx e^{(0)} + \epsilon e^{(1)} = e^{eq} - \tau \epsilon \boldsymbol{v} \cdot \nabla_0 e^{eq} = e^{eq} - \tau \boldsymbol{v} \cdot \nabla e^{eq}, \tag{A.10}$$

which is used in the discussion on the AP property of the DUGKS in the diffusive limit, i.e., Eq. (50).

Appendix B. The implicit step and explicit second-order upwind schemes

For brevity we present the two schemes in one-dimensional case with a uniform mesh. The implicit step scheme can be expressed as [35],

$$\frac{\phi_{\alpha j}^{n+1} - \phi_{\alpha j}^{n}}{\Delta t} + v_g \mu \frac{\phi_{\alpha,j+1/2}^{n+1} - \phi_{\alpha,j-1/2}^{n+1}}{\Delta x} = -\frac{1}{\tau_j}\left[\phi_{\alpha j}^{n+1} - \phi_{\alpha}^{eq}(E_j^{n+1})\right], \tag{B.1}$$

where $\phi_{\alpha,j+1/2}$ is the energy distribution function at the interface between cell j and $j+1$, which is given by

$$\phi_{\alpha,j+1/2} = \begin{cases} \phi_{\alpha,j} & \mu > 0, \\ \phi_{\alpha,j+1} & \text{else}. \end{cases} \tag{B.2}$$

As shown in [35], the implicitness in the term $\phi_{\alpha}^{eq}(E_j^{n+1})$ requires an iterative procedure to solve Eq. (B.3) at each time step, i.e., an inner iteration is implemented as

$$\frac{\phi_{\alpha j}^{n+1,k} - \phi_{\alpha j}^{n}}{\Delta t} + v_g \mu \frac{\phi_{\alpha,j+1/2}^{n+1,k} - \phi_{\alpha,j-1/2}^{n+1,k}}{\Delta x} = -\frac{1}{\tau_j}\left[\phi_{\alpha j}^{n+1,k} - \phi_{\alpha}^{eq}(E_j^{n+1,k-1})\right], \tag{B.3}$$

for $k = 1, 2, \ldots$, with $E_j^{n+1,0} = E_j^n$. As the iteration convergent ($k = k_\infty$), we set $\phi_{\alpha j}^{n+1} = \phi_{\alpha j}^{n+1,k_\infty}$ and the calculation advances to the new time step. The convergence criterion is chosen as the relative error of the energy density between two steps is less than 10^{-6}, which can ensure a convergent solution. The explicit second-order upwind (2nd-Upwind) scheme reads,

$$\frac{\phi_{\alpha j}^{n+1} - \phi_{\alpha j}^{n}}{\Delta t} + v_g \mu \frac{\phi_{\alpha,j+1/2}^{n} - \phi_{\alpha,j-1/2}^{n}}{\Delta x} = -\frac{1}{\tau_j}\left[\phi_{\alpha j}^{n} - \phi_{\alpha}^{eq}(E_j^{n})\right], \tag{B.4}$$

where the cell interface distribution function is reconstructed as

$$\phi_{\alpha,j+1/2} = \begin{cases} \phi_{\alpha,j} + \delta_j \phi_{\alpha,j}(x_{j+1/2} - x_j) & \mu > 0, \\ \phi_{\alpha,j+1} - \delta_{j+1}\phi_{\alpha,j+1}(x_{j+1} - x_{j+1/2}) & \text{else}, \end{cases} \tag{B.5}$$

where $\delta_j \phi_{\alpha,j}$ is the slope of ϕ_{alpha} at cell j, which can be calculated using the central-difference or van Leer limiter methods as given by Eqs. (31) and (32). We found the central-difference reconstruction will produce unphysical oscillations, and therefore the van Leer limiter is employed in our simulations. As an explicit method, the time step of the 2nd-Upwind method should satisfy the CFL condition.

References

[1] J.Y. Murthy, S. Narumanchi, J.A. Pascual-Gutierrez, et al., Review of multiscale simulation in submicron heat transfer, Int. J. Multiscale Computat. Eng. 3 (2005) 5–32.

[2] A.J. Minnich, Advances in the measurement and computation of thermal phonon transport properties, J. Phys.: Condens. Matter 27 (2015) 053202.

[3] G. Chen, Nanoscale Energy Transport and Conservation, Oxford University Press, 2005.

[4] Y.Y. Guo, M.R. Wang, Phonon hydrodynamics and its applications in nanoscale heat transport, Phys. Rep. 595 (2015) 1–44.

[5] E.W. Larsen, J.E. Morel, Advances in discrete-ordinates methodology, in: Y. Azmy, E. Sartori (Eds.), Nuclear Computational Science: A Century in Review, Springer, 2010, pp. 1–84.

[6] R.B. Peterson, Direct simulation of phonon-mediated heat transfer in a debye crystal, J. Heat Transfer 116 (1994) 815–822.

[7] S. Mazumder, A. Majumdar, Monte Carlo study of phonon transport in solid thin films including dispersion and polarization, J. Heat Transfer 123 (2001) 749–759.

[8] J.P.M. Péraud, N.G. Hadjiconstantinou, Efficient simulation of multidimensional phonon transport using energy-based variance-reduced Monte Carlo formulations, Phys. Rev. B 84 (2011) 205331.

[9] F. Liu, H.A. Becker, A. Pollard, Spatial differencing schemes of the discrete-ordinates method, Numer. Heat Transfer B 30 (1996) 23–43.

[10] S.A. Ali, G. Kollu, S. Mazumder, et al., Large-scale parallel computation of the phonon Boltzmann transport equation, Int. J. Therm. Sci. 86 (2014) 341–351.

[11] N. Donmezer, S. Graham, A multiscale thermal modeling approach for ballistic and diffusive heat transport in two dimensional domains, Int. J. Therm. Sci. 76 (2014) 235–244.

[12] Y. Zhang, W. Ye, Modified ballistic-diffusive equations for transient non-continuum heat conduction, Int. J. Heat Mass Transfer 83 (2015) 51–63.

[13] S. Hamian, T. Yamada, M. Faghri, K. Park, Finite element analysis of transient ballistic-diffusive phonon heat transport in two-dimensional domains, Int. J. Heat Mass Transfer 80 (2015) 781–788.

[14] Z.L. Guo, C. Shu, Lattice Boltzmann Method and its Applications in Engineering, World Scientific Publishing, 2013.

[15] D.P. Sellan, J.E. Turney, A. McGaughey, C.H. Amon, Cross-plane phonon transport in thin films, J. Appl. Phys. 108 (2010) 113524.

[16] M. Xu, Q. Chen, Temperature enhancement through interaction of thermal waves for phonon transport in silicon thin films, Int. J. Thermophys. 34 (2013) 306–321.

[17] A. Christensen, S. Graham, Multiscale lattice Boltzmann modeling of phonon transport in crystalline semiconductor materials, Numer. Heat Transfer B 57 (2010) 89–109.

[18] Y.Y. Guo, M.R. Wang, Lattice Boltzmann modeling of phonon transport, J. Comput. Phys. 315 (2016) 1–15.

[19] N. Zuckerman, J.R. Lukes, Combined kinetic Monte Carlo-molecular dynamics approach for modeling phonon transport in quantum dot superlattices, J. Heat Transfer 136 (2014) 012401.

[20] A. Chattopadhyay, A. Pattamatta, A Comparative study of submicron phonon transport using the Boltzmann transport equation and the lattice Boltzmann method, Numer. Heat Transfer Part B 66 (2014) 360–379.

[21] Z.L. Guo, K. Xu, R.J. Wang, Discrete unified gas kinetic scheme for all Knudsen number flows: low-speed isothermal case, Phys. Rev. E 88 (2013) 033305.

[22] Z.L. Guo, R.J. Wang, K. Xu, Discrete unified gas kinetic scheme for all Knudsen number flows. II. Thermal compressible case, Phys. Rev. E 91 (2015) 033313.

[23] L.H. Zhu, Z.L. Guo, K. Xu, Discrete unified gas kinetic scheme on unstructured meshes, Comput. Fluids 127 (2016) 211–225.

[24] P. Wang, L.H. Zhu, Z.L. Guo, K. Xu, A comparative study of LBE and DUGKS methods for nearly incompressible flows, Comm. Comput. Phys. 17 (2015) 657–681.

[25] L.H. Zhu, P. Wang, Z.L. Guo, Performance evaluation of the general characteristics based off-lattice Boltzmann and DUGKS methods for low speed continuum flows: a comparative study, Fluid Dyn. (2015). arXiv preprint arXiv: 1511.00242.

[26] D.G. Cahill, P.V. Braun, G. Chen, et al., Nanoscale thermal transport. II. 2003–2012, Appl. Phys. Rev. 1 (2014) 011305.

[27] J.M. Ziman, Electrons and Phonons, Oxford University Press, 1960.

[28] A. Majumda, Microscale heat conduction in dielectric thin films, ASME J. Heat Transfer 15 (1993) 7–16.

[29] K. Xu, J.-C. Huang, A unified gas-kinetic scheme for continuum and rarefied flows, J. Comput. Phys. 229 (2010) 7747–7764.

[30] L. Mieussens, On the asymptotic preserving property of the unified gas kinetic scheme for the diffusion limit of linear kinetic models, J. Comput. Phys. 253 (2013) 138–156.

[31] B. van Leer, Towards the ultimate conservative difference scheme. IV. A new approach to numerical convection, J. Comput. Phys. 23 (1977) 276–299.

[32] S.V. Narumanchi, J.Y. Murthy, C.H. Amon, Simulation of unsteady small heat source effects in sub-micron heat conduction, ASME J. Heat Transfer 125 (2003) 896–903.

[33] M.J. Fryer, H. Struchtrup, Moment model and boundary conditions for energy transport in the phonon gas, Continuum Mech. Thermodyn. 26 (2014) 593–618.

[34] W. Fiveland, The selection of discrete ordinates quadrature sets for anisotropic scattering, Fund. Rad. Heat Transfer, ASME HTD 160 (1991) 89–96.

[35] R. Yang, G. Chen, M. Laroche, Y. Taur, Multidimensional transient heat conduction at nanoscale using the ballistic-diffusive equations and the Boltzmann equation, J. Heat Transfer 127 (2005) 298–306.

[36] M. Abramowitz, I.A. Stegun, Handbook of Mathematical Functions, Dover Publications, 1965.

[37] N. Hale, A. Townsend, Fast and accurate computation of Gauss–Legendre and Gauss–Jacobi quadrature nodes and weights, SIAM J. Sci. Comput. 35 (2013) A652–A674.
[38] Q. Hao, G. Chen, M.-S. Jeng, Frequency-dependent Monte Carlo simulations of phonon transport in two-dimensional porous silicon with aligned pores, J. Appl. Phys. 106 (2009) 114321.
[39] A.J. Minnich, Determining phonon mean free paths from observations of quasiballistic thermal transport, Phys. Rev. Lett. 109 (2012) 205901.
[40] K.C. Collins, A.A. Maznev, Z. Tian, et al., Non-diffusive relaxation of a transient thermal grating analyzed with the Boltzmann transport equation, J. Appl. Phys. 114 (2013) 104302.
[41] I.A. Kotsireas, A Survey on Solution Methods for Integral Equations, Ontario Research Centre for Computer Algebra Technical Report 47, 2008.
[42] A.L. Crosbie, R.G. Schrenker, Radiative transfer in a two-dimensional rectangular medium exposed to diffuse radiation, J. Quant. Spectrosc. Radiat. Transfer 31 (1984) 339–372.
[43] Y. Sone, Kinetic Theory and Fluid Dynamics, Birkhäuser, 2002.
[44] L. Mieussens, On the asymptotic preserving property of the unified gas kinetic scheme for the diffusion limit of linear kinetic models, J. Comput. Phys. 253 (2013) 138–156.